
Climate Data Record (CDR) Program

Climate Algorithm Theoretical Basis Document (C-ATBD)

The Development of Advanced Microwave Sounding Unit (AMSU) and Microwave Humidity Sounder (MHS) Fundamental Climate Data Records (FCDR) for Hydrological Applications

C-ATBD: AMSU-A Brightness Temperature



CDR Program Document Number: CDRP-ATBD-0798
Configuration Item Number: 01B-38a
Revision 1 / May 5, 2016

REVISION HISTORY

Rev.	Author	DSR No.	Description	Date
1	Ralph Ferraro, Huan Meng, NOAA/NESDIS/STAR Wenze Yang UMD/ESSIC/CICS	DSR-1000	Initial Submission to CDR Program	05/05/2016

TABLE of CONTENTS

1. INTRODUCTION.....	7
1.1 Purpose	7
1.2 Definitions	7
1.3 Referencing this Document.....	8
1.4 Document Maintenance	8
2. OBSERVING SYSTEMS OVERVIEW.....	9
2.1 Products Generated	10
2.2 Instrument Characteristics	10
3. ALGORITHM DESCRIPTION.....	12
3.1 Algorithm Overview	12
3.2 Processing Outline	12
3.2.1 Reading Input.....	12
3.2.2 Geolocation Correction.....	12
3.2.3 Inter-satellite Correction	12
3.2.4 Calculating Radiance	13
3.2.5 Generating Brightness Temperatures.....	14
3.2.6 Scan Bias Corrections.....	14
3.2.7 Quality Control.....	14
3.2.8 Writing Output.....	15
3.3 Algorithm Input	15
3.3.1 Primary Sensor Data	15
3.3.2 Ancillary Data.....	15
3.3.3 Derived Data	15
3.3.4 Forward Models.....	16
3.4 Theoretical Description	16
3.4.1 Physical and Mathematical Description.....	16
3.4.2 Data Merging Strategy	25
3.4.3 Numerical Strategy	26
3.4.4 Calculations.....	26
3.4.5 Look-Up Table Description.....	26
3.4.6 Parameterization	27
3.4.7 Algorithm Output.....	27
4. TEST DATASETS AND OUTPUTS.....	28
4.1 Test Input Datasets	28
4.2 Test Output Analysis	28
4.2.1 Reproducibility	28
4.2.2 Precision and Accuracy	28
4.2.3 Error Budget.....	30

5. PRACTICAL CONSIDERATIONS.....	31
5.1 Numerical Computation Considerations	31
5.2 Programming and Procedural Considerations	31
5.3 Quality Assessment and Diagnostics.....	31
5.4 Exception Handling	31
5.4.1 Conditions Checked	31
5.4.2 Conditions Not Checked	32
5.4.3 Conditions Not Considered Exceptions.....	32
5.5 Algorithm Validation.....	32
5.5.1 Geolocation Correction.....	32
5.5.2 Scan Bias Correction	34
5.5.3 Inter-Satellite Calibration.....	35
5.6 Processing Environment and Resources.....	35
6. ASSUMPTIONS AND LIMITATIONS	36
6.1 Algorithm Performance	36
6.2 Sensor Performance.....	36
7. FUTURE ENHANCEMENTS.....	38
7.1 Enhancement 1 – Extension of NOAA-15 FCDR Record	38
7.2 Enhancement 2 – Correction of Frequency Shift	38
7.3 Enhancement 3 – Inter-Satellite Calibration over Land	38
7.4 Enhancement 4 – Improving Cross Scan Asymmetry Correction.....	38
8. REFERENCES.....	39
APPENDIX A. ACRONYMS AND ABBREVIATIONS.....	40
APPENDIX B. AMSU-A SENSOR DETAILS.....	42
APPENDIX C. SAMPLE AMSU-A FCDR FILE FORMAT.....	45

LIST of FIGURES

Figure 1: Equatorial crossing times (LST) for NOAA-15 through NOAA-19, as well as MetOp-A (20). This is for ascending nodes.....	9
Figure 2: AMSU-A scan geometry.....	11
Figure 3: AMSU-A FCDR processing flow chart.....	13
Figure 4: Schematic explanation of the geolocation correction method	17
Figure 5: Iterative search for μ_{N15} of 23.8 GHz channel.....	20
Figure 6: Tropical ocean 15-day mean Tb and Δ Tb for 23.8 and 30.4 GHz channels. Left and right panels are respectively for before and after inter-calibration correction.	22
Figure 7: Tropical ocean mean Tb and Δ Tb for 50.3 and 89.0 GHz channels. Left and right panels are respectively for before and after inter-calibration correction.	23
Figure 8: Mean difference between the simulated and the observed NOAA-15 AMSU-A brightness temperatures under clear-sky over ocean in mid- and low-latitude, (a) 23.8, (b) 31.4, (c) 50.3 and (d) 89 GHz. Results are for all observation (All), most probable value stratification (MPV), and vicarious cold reference (VCR). The mean bias is relative to nadir.	24
Figure 9: Mean difference between simulated and observed NOAA-15 AMSU-A brightness temperatures at 23.8, 31.4, 50.3 and 89 GHz over Amazon and under clear sky.	24
Figure 10: Similar to Figure 8, after the three-point bias correction.....	25
Figure 11: Time series of the satellite attitudes for NOAA-15 AMSU-A 23.8 GHz (channel 1). AMSU-A2 instrument is mounted about 1.2 degrees negative cross-track, so the sensor does not point to the nadir when the scan angle is zero. The sensor has a small along track offset as well, about 0.5 degree.	33
Figure 12: Difference between ascending and descending brightness temperatures from NOAA-15 AMSU-A 23.8 GHz channel, (a) before correction; (b) after correction.	34
Figure 13: Geographical distribution of cloud liquid water (upper panels) and land surface emissivity at 31.4 GHz (lower panels), derived through MSPPS. Images (a) and (c) are the original products; and (b) and (d) are with scan bias correction. For clarity, the 31.4 GHz emissivity is shown over the continent of Africa instead of the entire globe.	35
Figure 14: Time series of NOAA-16 channel 3 brightness temperature before (black) and after (blue) de-trending.....	36

LIST of TABLES

Table 1: AMSU-A product attributes.....	10
Table 2: AMSU-A Sensor Geolocation Error (km)/LZA error (deg)	17
Table 3: Optimal μ , δR , and κ	20
Table 4: Standard Deviation of ΔT_b over Tropical Ocean	23
Table 5: ΔT_b (K) of Brightness Temperature Difference between Satellite Pairs	29
Table 6: Asymmetry Index (K) of AMSU-A Window Channels	29
Table 7: Error Budget of AMSU-A Window Channels FCDR.....	30

1. Introduction

1.1 Purpose

The purpose of this document is to describe the algorithm submitted to the National Climatic Data Center (NCDC) by Ralph Ferraro and Huan Meng, Co-Principal Investigators from the NOAA/NESDIS/Center for Satellite Applications and Research (STAR), that will be used to create the Advanced Microwave Sounding Unit-A (AMSU-A) brightness temperature Fundamental Climate Data Record (FCDR) for “window channels” that are useful for hydrological product Thematic CDR (TCDR). The AMSU-A sensor is flown on NOAA-15, -16, -17, -18, -19 and MetOp-A satellites (note the MetOp-B satellite was launched in 2012 but is not included in this data set). The actual algorithm is defined by the computer program (code) that accompanies this document, and thus the intent here is to provide a guide to understanding that algorithm, from both a scientific perspective and in order to assist a software engineer or end-user performing an evaluation of the code.

1.2 Definitions

Directional parameters:

$$\alpha, \beta, a_0, \text{ and } a_1 = \text{SNO coefficients} \quad (1)$$

Radiative parameters:

$$\text{Level-1C calibration equation: } R = R_L + \delta R + \mu Z \quad (2)$$

$R = \text{Earth scene radiance}$

$R_L = \text{Earth scene radiance from the linear calibration}$

$\delta R = \text{Calibration offset (determined by post-launch calibration)}$

$\mu = \text{Non-linear calibration coefficient (determined by post-launch calibration)}$

$Z = \text{Non-linear response}$

$$\text{Scan asymmetry: } A_i = \Delta TB_i - \frac{\Delta TB_{15} + \Delta TB_{16}}{2} \quad (3)$$

$A_i = \text{Scan asymmetry}$

$TB_i = \text{Brightness temperature at beam position } i$

$\Delta TB_i = \text{Difference between simulated and observed brightness temperature}$

1.3 Referencing this Document

This document should be referenced as follows:

AMSU-A Brightness Temperature - Climate Algorithm Theoretical Basis Document, NOAA Climate Data Record Program CDRP-ATBD-0798 Rev. 1 (2016). Available at <http://www.ncdc.noaa.gov/cdr/fundamental>

1.4 Document Maintenance

The algorithm used to generate the FCDR's consists of two primary components. The first is associated with the sensor characterization for each satellite used in the time series. Within this component, there are various subsystems that are used to perform sensor bias corrections and geolocation corrections. These are typically run "off line" as more of a development effort and is not envisioned to be changed very frequently (in fact, this function could still be carried out by the PI team as part of their stewardship activities to extend the time series with recently launched satellites and newer sensors such as MetOp-B or JPSS/ATMS). However, if improvement within the process changes over time to upgrade the maturity of the CDR, the C-ATBD will be updated. Additionally, several of these algorithms are documented in the open literature; the C-ATBD will also be updated when new publications are generated.

The second change is associated with intersatellite calibration and time series extension and reprocessing after transition to NCDC. In this case, it is envisioned that updated corrections, most likely in the form of look up tables of coefficients and derived data, would be delivered to the CDR program and those tables updated within the C-ATBD.

Synchronization between this document and the algorithm is achieved through version and revision numbers, i.e., there will be consistency between the version numbers on the front cover of this document and the version and revision numbers contained within the FCDR software itself (i.e., various header files within the software documentation).

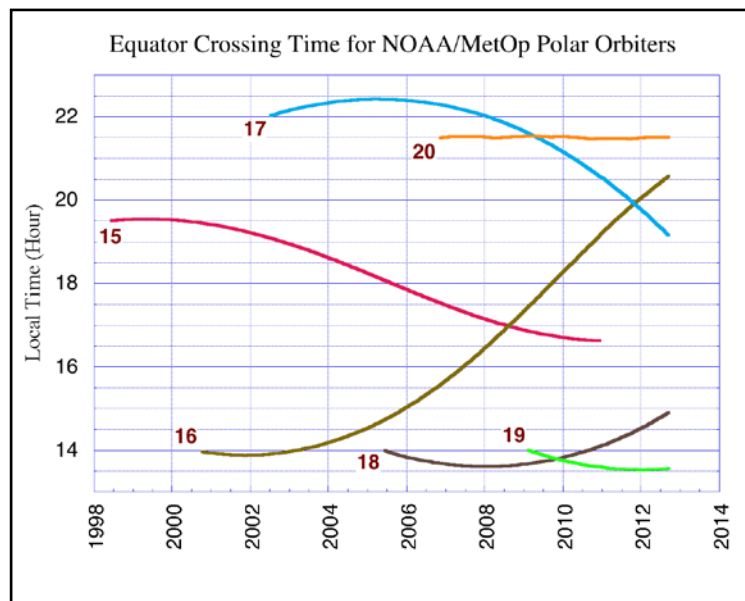
2. Observing Systems Overview

This section provides an overview of the characteristics of the AMSU-A observing systems and its calibration strategy. For more specific details on the AMSU-A sensor, please refer to Appendix B.

The AMSU-A sensor was designed to enhance the vertical profiling of temperature to support NOAA's operational mission. In this manner, it is used in conjunction with the AMSU-B (later on Microwave Humidity Sounder or MHS) and HIRS sensor as part of the ATOVS system; this is substantial upgrades to their predecessors, the MSU and SSU sensors. The first AMSU-A was flown on the NOAA-15 satellite in July 1998; subsequent sensors have been flown on NOAA-16, -17, -18 and -19 satellites, as well as the MetOp-A and most recently (September 2012), MetOp-B. Figure 1 shows the complete set of the satellites used in this CDR project (which covers the period 2000 through 2010), their period of records, and their time of local ascending overpass.

In addition to the legacy TOVS products and MSU climate time series which primarily utilize "sounding" channels in the oxygen (50-60 GHz) and water vapor (183 GHz) absorption bands, and based on heritage from the DMSP SSM/I series, NOAA began to use the AMSU-A and -B window channels (initially included for surface and precipitation screening) generating "Hydrological Products" (e.g., rain rate, snow cover, sea-ice concentration, etc.) from NOAA-15 through the Microwave Surface and Precipitation Products System (MSPPS; Ferraro et al. 2005). These products have gained increasing popularity in both the operational weather and climate communities, thus, the motivation for this project. It should be noted that an independent CDR project – MSU/AMSU Radiance FCDR's – focuses on the AMSU-A sounding channels above 50 GHz.

Figure 1: Equatorial crossing times (LST) for NOAA-15 through NOAA-19, as well as MetOp-A (20). This is for ascending nodes.



2.1 Products Generated

The primary data sets generated from this algorithm is a swath level-1c (L1C) brightness temperature (T_b), henceforth denoted as the FCDR, of the AMSU-A channel 1,2,3 and 15 (23.8, 31.4, 50.3 and 89 GHz). Further details are provided in Table 1. The initial data set covers the time period from January 2000 – December 2010. The data are stored in netCDF version 4.0 files that include the necessary metadata and supplementary data fields which are described in detail in Section 3.4.7.

Table 1: AMSU-A product attributes

Parameter	Attribute
Satellite/Period of Record	NOAA-15/Jan 1, 2000 – Dec 31, 2010 NOAA-16/Jan 1, 2001 – Dec 31, 2010 NOAA-17/Jun 29, 2002 – Dec 31, 2010 (for channels 3 and 15: Jun 29, 2002 – Oct 27, 2003) NOAA-18: May 25, 2005 – Dec 31, 2010 NOAA-19: Feb 7, 2009 – Dec 31, 2010 MetOp-A: Jan 1, 2007 – Dec 31, 2010
Geographic Coverage	Global (2343 km swath width)
Spatial Resolution	48 x 48 km nadir; 79 x 147 km at limb
Channels	1,2,3 and 15
Channel Frequency	23.8, 31.4, 50.3, and 89.0
Precision & Accuracy (K)	Varies with satellite and channel. See Section 4.2.2

2.2 Instrument Characteristics

The Advanced Microwave Sounding Unit-A (AMSU-A) is cross-track scanning sensor designed to measure earth scene radiances; its primary design function is to provide temperature profiling of the atmosphere. AMSU-A was first flown on the NOAA-15 satellite (July 1998); it is substantial upgrades to its predecessor, MSU in terms of the number of channels (15 vs. 5), instrument precision, and spatial resolution. The most complete references to the sensor can be found in Kidwell (1998), and Robel et al. (2009), whereas further information is provided in Appendix B.

AMSU-A is a multi-channel microwave radiometer that will be used for measuring global atmospheric temperature profiles. It provides information on atmospheric water in all of its forms (with the exception of small ice particles, which are

transparent at microwave frequencies). AMSU-A provides information even in cloudy conditions.

AMSU-A is designed to measure scene radiances in 15 discrete frequency channels (23-90 GHz). At each channel frequency, the antenna beam width is a constant 3.3 degrees (at the half power point). Thirty consecutive scene resolution cells are sampled in a stepped-scan fashion every eight seconds, each scan covering about 50 degrees on either side of the sub-satellite path.

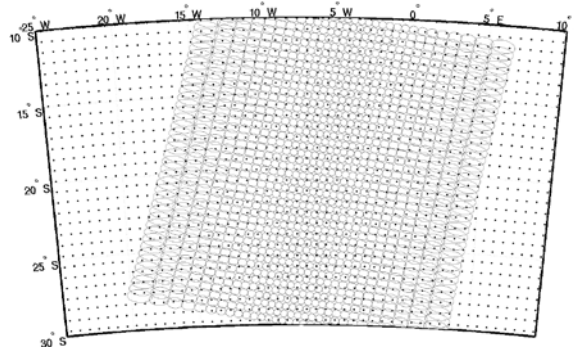


Figure 2: AMSU-A scan geometry.

These scan patterns and geometric resolution translate to a 48 km diameter cell at nadir and a 2,343 km swath width from the 837 km nominal orbital altitude (see Figure 2). AMSU-A uses oxygen absorption bands/lines for atmospheric temperature sounding. Window channels at 23.8, 31.4 and 89 GHz provide information on surface temperature and emissivity over land, and precipitable water, cloud water and sea-ice cover over water.

Hardware for the two lowest frequencies is located in one module (AMSU-A2), with the remaining 13 frequencies being accommodated in the second module (AMSU-A1). This arrangement puts the two lower atmospheric moisture viewing channels into one module and the oxygen absorption channels into a second common module, in order to ensure commonality of viewing angle (independent of any module and/or spacecraft misalignment due to structural or thermal distortions). The AMSU-A2 module has a single antenna assembly, providing data for channels 1 and 2. AMSU-A1 has two separate antenna assemblies: AMSU-A1.1 provides data for channels 6,7 and 9-15 and AMSU-A1.2 provides data for channels 3, 4, 5 and 8.

3. Algorithm Description

3.1 Algorithm Overview

This section describes the generation of the FCDR's for the AMSU-A channels described in Table 1. It provides details on the geolocation correction, the scan bias correction and the intersatellite calibration, which are the three main steps to convert the original AMSU-A Level-1B (L1B) data to AMSU-A FCDR's. There are other intermediate steps such as the conversion from antenna to brightness temperature, the generation of look up table parameters (that are part of an off-line system) and quality control that are part of the FCDR algorithm. Specific details are provided in the sections below.

3.2 Processing Outline

The steps of the AMSU-A FCDR algorithms include reading the input data (L1B), processing the data in six steps (described in following sections), and the writing of the output data (FCDR). The processing flow is shown in Figure 3. Note that the steps for generating Thematic CDR's (TCDR) are not included in this C-ATBD.

3.2.1 Reading Input

The operational system first reads all the input data which include primary sensor data (including earth scene count, warm count, and cold count from AMSU-A L1B data), ancillary data (including land-sea mask, GFS data, etc.), and derived data (including various correction coefficients, and new geolocation dataset). These data will be described in more details in Sections 3.3.1-3.

3.2.2 Geolocation Correction

Geolocation has been corrected offline, and a new geolocation dataset, including latitude, longitude, scan angle, and EIA, has been developed. The operational system reads the new geolocation dataset and uses the data in the remaining tasks without further processing of the geolocation data. More details on geolocation correction are described in 3.4.1.1.

3.2.3 Inter-satellite Correction

The inter-satellite calibration coefficients, including inter-satellite radiance offset δR , nonlinearity coefficient μ , and changing slope k , for each channel and each onboard satellite, has been calculated offline. The operational system uses the coefficients to calculate corrected radiances. More details on how these coefficients are calculated are described in 3.4.1.2.

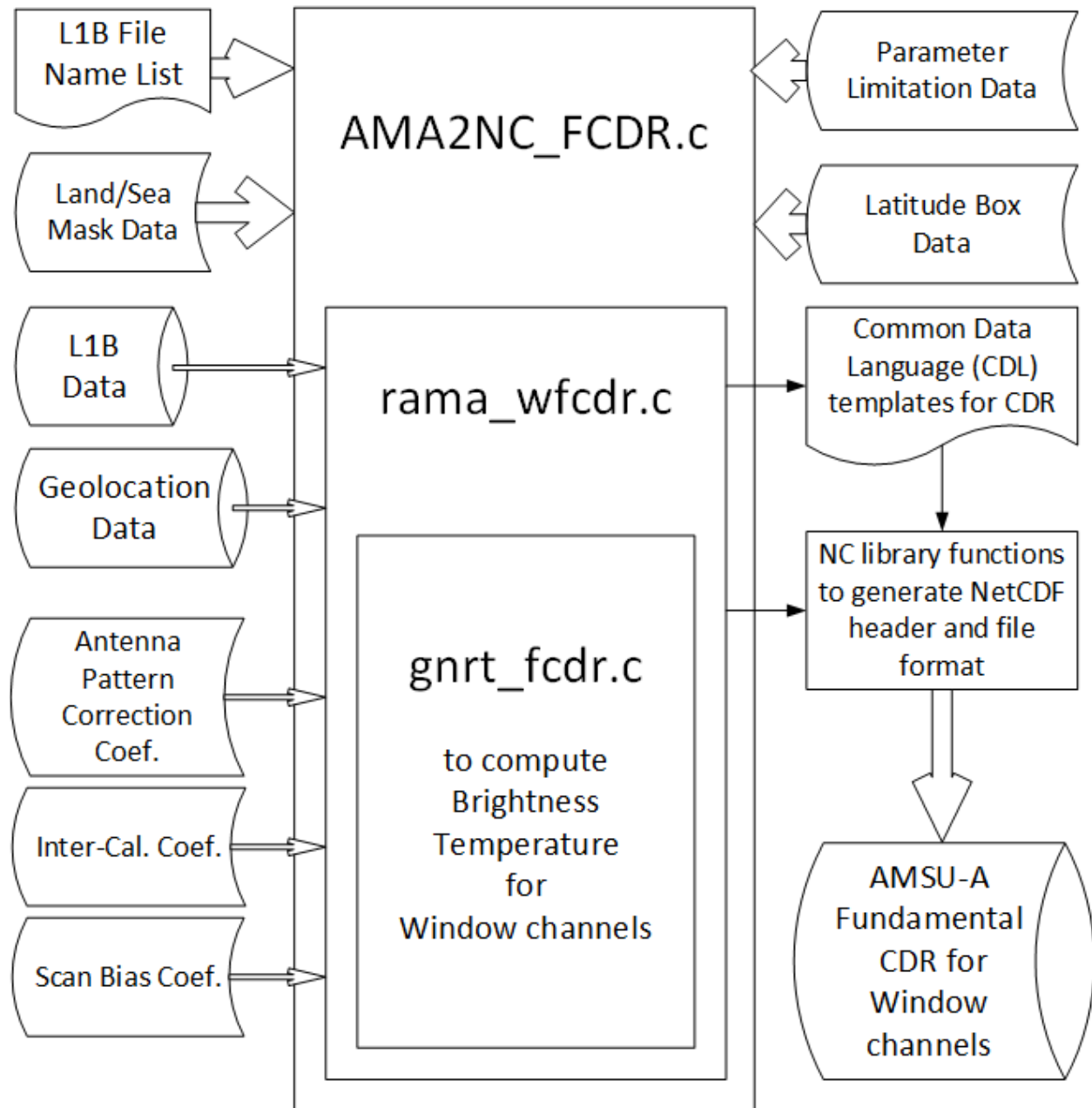


Figure 3: AMSU-A FCDR processing flow chart

3.2.4 Calculating Radiance

Radiance is usually calculated from the combination of earth scene count (C_e) and the accompanying count-to-radiance conversion coefficients, pre-calculated and stored in the L1B data set, and then an antenna pattern correction is performed. However, these count-to-radiance conversion coefficients are no longer valid in the current operational system. This project adopts the Integrated Microwave Inter-Calibration Approach (IMICA) (Zou et al, 2006, 2009, 2010 and 2011) for inter-satellite calibration for the AMSU-A

window channels. IMICA requires that calibration starts from the count of warm target (C_w) and cold target (C_c), as shown in Equation (3-5) to (3-7). The end result is a new set of calibration coefficients including updated nonlinearity coefficient μ , and a new inter-satellite radiance offset δR (Eq. (3-4)). The coefficients are employed in the operational system to compute inter-satellite corrected radiances from counts.

3.2.5 Generating Brightness Temperatures

After calculating the radiances, the antenna pattern correction is applied to each channel, then the brightness temperatures are generated by applying Planck function with the central frequencies of specified channels.

3.2.6 Scan Bias Corrections

The scan bias correction coefficients, including three polynomial coefficients for each beam position, each channel and each onboard satellite, has been calculated offline. The operational system uses the coefficients to calculate the scan bias and correct brightness temperature. More details on how these coefficients are calculated are described in 3.4.1.3.

3.2.7 Quality Control

Currently, the quality flag is recorded for each scan line and each channel. The descriptions of each bit from high to low are as follow:

Bit 7: Inherited from L1B test bit 31 of Quality Indicator Bit Field, if the bit is on (=1), it indicates do not use scan for product generation;

Bit 6: Calibration issues, including bad blackbody view counts, bad space view counts, or bad PRTs for this scan line;

Bit 5: Time field is bad or problematic;

Bit 4: Earth location is questionable, or no earth located because of bad time; note the indication of this field mostly refers to error in the original L1B data although the FCDR processing system also updates the flag in some cases;

Bit 3: Calculated brightness temperature is out of expected range;

Bit 2: Lunar contamination was detected in the space view counts of this channel, and has been corrected when used in the calibration;

Bit 1: Reserved for future expansion;

Bit 0: Reserved for future expansion.

In addition to using quality flag to indicate quality issues in the FCDR data, a very small number of L1B data files were removed from the FCDR data set due to time errors that were not flagged in the L1B data.

3.2.8 Writing Output

The calculation results and meta information are written out in NetCDF4 format. Information such as conventions, title, and product version etc. is recorded in the attribute fields. In the data fields, variables are divided into two groups: data, and geolocation and time. In the data group, the recorded variables are orbital mode, surface type, earth incidence angle, solar zenith angle, and FCDR brightness temperatures. Data in the geolocation and time group include latitude, longitude, scan time, and scan time since 1998.

Note that, since the AMSU-A window channels are located on three modules, i.e. 23.8 GHz and 31.4 GHz on AMSU-A2, 50.3 GHz on AMSU-A1-2, and 89 GHz on AMSU-A1-1 (Section 2.2.1), and each module has unique corrections, there are three sets of geolocation variables in the FCDR including earth incidence angles, scan angle, latitude, and longitude.

3.3 Algorithm Input

3.3.1 Primary Sensor Data

The primary sensor data for AMSU Hydrology FCDR is L1B AMSU-A data (Note: AMSU-B and MHS L1B data are also required for generating the complete set of AMSU Hydrology FCDR. However, the descriptions of the AMSU-B and MHS FCDR are not included in this document but in a separate C-ATBD.). The generic L1B data, accessible from NOAA Comprehensive Large Array-data Stewardship System (CLASS), keep orbital records of these cross-scan sensors in binary format with approximately 14 files per day. AMSU-A has a resolution of 48x48 kilometers at nadir view, and 150x80 kilometers at outer most beam position. The data size is 9.9 GB per satellite year with a total data size of 415 GB for all satellites and all available years. More descriptions of this data set is referred to Robel et al., (2009), KLM user's guide.

3.3.2 Ancillary Data

The production package requires a land-sea mask. The binary data is on a 1/16 degree gridded map with cylindrical projection. The size of the map is about 16 MB. The file is located in directory .../amsua-fcdr/input.

3.3.3 Derived Data

The operational system requires the following derived data: corrected geolocation data, inter-satellite calibration coefficients, antenna pattern correction (APC) coefficients, scan bias correction coefficients.

Geolocation (latitude, longitude, earth incidence angle, and scan angle) is corrected following the approach described in 3.4.1.1 (Moradi et al, 2013). The corrected geolocation data is 5.6 GB per satellite year with a total size of 213 GB for all satellites and all available years. The files are under .../amsua-fcdr/input directory.

The AMSU-A inter-satellite calibration coefficients, including inter-satellite radiance offset δR , nonlinearity coefficient μ , and changing slope k , for each channel and

each onboard satellite, is stored in a text file with the size of 1 KB. This file, `mu_dr_k.dat`, is provided under `.../amsua-fcdr/input` directory. The derivation of the data is described in 3.4.1.2.

The AMSU-A antenna pattern correction (APC) coefficients, including antenna efficiencies over earth f_e , satellite platform f_{sat} , and cold space f_c for each beam position and each channel, and the scale factor η for each channel, is stored in a text APC file. Every satellite has one APC file with the size of 3 KB. The files are provided under `.../amsua-fcdr/input` directory. The derivation of the data is described in Mo (1999).

The AMSU-A scan bias correction (ASYM) coefficients, including three polynomial coefficients for each beam position and each channel, is stored in a text ASYM file. Every satellite has one ASYM file with the size of 6 KB. The files are provided under `.../amsua-fcdr/input` directory. The derivation of the data is described in 3.4.1.3 (Yang et al., 2013).

3.3.4 Forward Models

Not applicable.

3.4 Theoretical Description

3.4.1 Physical and Mathematical Description

3.4.1.1 Geolocation Correction

The geolocation has been corrected for all AMSU-A sensors aboard the NOAA Polar-orbiting Operational Environmental Satellites (POES) satellites (NOAA-15 to -19). The correction algorithm is schematically explained in Figure 4.

The results show that NOAA-15 AMSU-A2 sensor is mounted about 1.2 degrees negative cross track, and about 0.5 degree positive along track. NOAA-16 AMSU-A1 and -A2 are mounted about 0.5 degree positive along track, and NOAA-18 AMSU-A2 is mounted more than 1 degree positive along track. Table 2 gives the average geolocation error and the Earth Incidence Angle (EIA) error caused by geolocation problem for the AMSU-A sensors.

A new geolocation dataset has been developed for the AMSU-A instruments aboard NOAA POES satellites. The new dataset includes latitude, longitude, scan angle, and EIA. This dataset will be used throughout the project for scan bias correction and inter-calibration.

This geolocation correction method cannot be applied to MetOp-A data as the geometry of the MetOp-A orbit is different from NOAA satellites and our method introduces some extra geolocation error. In addition, our investigations show that the MetOp-A geolocation error is rather small, less than a few kilometers, and does not introduce large error in scan bias or LZA.

Detailed description of the geolocation correction algorithm, results, and discussion has been published in Moradi et al. (2013).

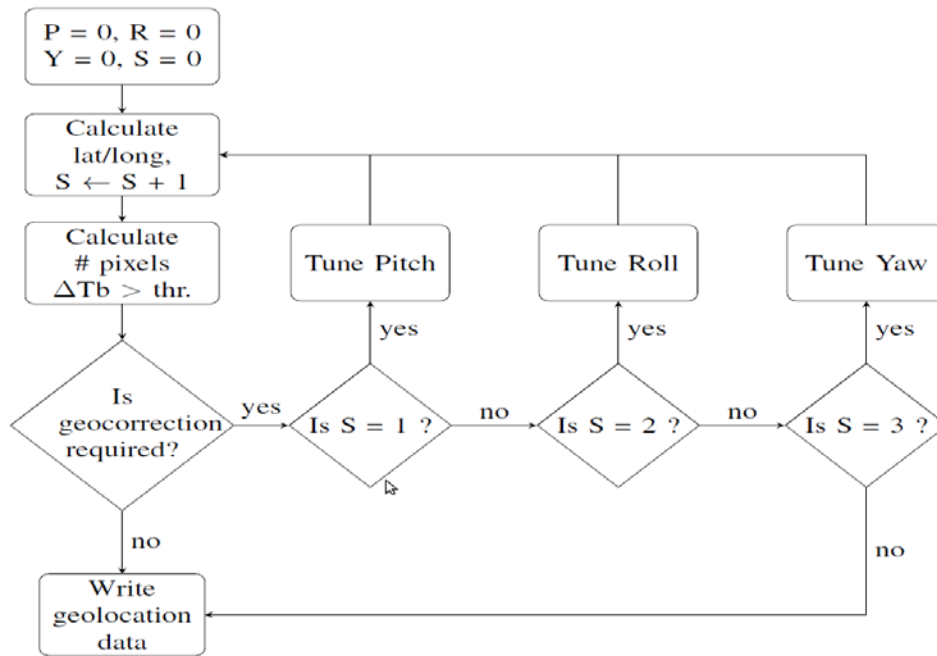


Figure 4: Schematic explanation of the geolocation correction method

Table 2: AMSU-A Sensor Geolocation Error (km)/LZA error (deg)

	AMSU-A2 ch1&2	AMSU-A1-2 ch3	AMSU-A1-1 ch15
NOAA-15	20/1.2	10/0.15	10/0.15
NOAA-16	10/0.25	10/0.4	10/0.2
NOAA-17	5-10/small	-*	-*
NOAA-18	20/0.2	5-10/small	5-10/0.4
NOAA-19	10/0.2	10/0.35	10/0.2

* NOAA-17 AMSU-A1 has a very short record due to instrument failure.

3.4.1.2 Inter-Satellite Calibration

Inter-satellite calibration has been conducted using simultaneous nadir overpass (SNO) and the IMICA approach. After identifying the threshold of standard deviation (STD) to quantify the homogeneity of SNO, we adopted Zou's IMICA method (Zou et al., 2006, 2009, 2010 and 2011) to correct for the warm target contamination and other problems. Warm target contamination is a major source of inter-satellite bias, and is difficult to correct with other approaches.

IMICA has been developed and applied to generate AMSU-A sounding channels FCDR. The basic procedure involves the following steps:

1. Generate intermediate SNO data set, which includes 142 variables for each SNO event;
2. Calculate SNO coefficients α , β , a_0 , and a_1 ;
3. Set $\delta R_{N15} = 0$, and μ_{N15} , calculate δR_k , μ_k , $k = 1$ to 5;
4. Generate Level-1C (L1C) radiances for all six satellites using recalibration coefficients;
5. Compute tropical ocean mean time series of Tb difference (ΔTb) between overlapping satellite pairs;
6. Change the value of μ_{N15} and repeat steps 3, 4, and 5;
7. Stop when summation of root mean square of ΔTb reaches minimum.

The basic equations are given below. Refer to Zou et al. (2006, 2009, 2010 and 2011) for the derivation of the equations.

$$I. \quad Z_j = \beta Z_k + \alpha + \zeta \quad (3-1)$$

$$II. \quad \begin{cases} \sum_{i=1}^N \Delta R_{L,i} = a_0 + a_1 \sum_{i=1}^N Z_{k,i} \\ \sum_{i=1}^N Z_{k,i} \Delta R_{L,i} = a_0 \sum_{i=1}^N Z_{k,i} + a_1 \sum_{i=1}^N Z_{k,i}^2 \end{cases} \quad (3-2)$$

$$III. \quad \begin{cases} a_0 = \Delta \delta R + \alpha \mu_j \\ a_1 = -\mu_k + \beta \mu_j \end{cases} \quad (3-3)$$

In which :

$$R = R_L - \delta R + \mu Z \quad (3-4)$$

$$R_L = R_c + S(C_e - C_c) \quad (3-5)$$

$$S = \frac{R_w - R_c}{C_w - C_c} \quad (3-6)$$

$$Z = S^2(C_e - C_c)(C_e - C_c) \quad (3-7)$$

where R is the Earth scene radiance, R_L represents the dominant linear response, R_c and R_w are radiance for cold space and warm target respectively, δR is a radiance offset; C_c , C_w and C_e are raw counts value of the satellite observations for cold space, warm target and the Earth view respectively; S is the slope determined by the two calibration targets; Z is a nonlinear response characterizing the nonperfect square law nature of a detector or a nonlinear amplifier; α and β are the offset and slope to describe the co-nonlinearity of the same sensor onboarding two different satellites, with subscription k referring to reference satellite, and j referring to other satellite; ζ represents the regression residual, assuming it is white noise; a_0 and a_1 are the least square coefficients.

The iterative adjustment of μ_{N15} can be illustrated in Figure 5. By setting μ_{N15} from -25 to 25 (sr m² cm⁻¹)(mW)⁻¹, δR_k and μ_k can be calculated as mentioned in step 3 above. Then a set of L1C radiances over the tropical ocean is generated, and compared with that of NOAA-15. Each satellite pair has a minimum STD of ΔT_b , and the δR_k and μ_k corresponding to the averaged minimum STD of ΔT_b from all satellites are selected.

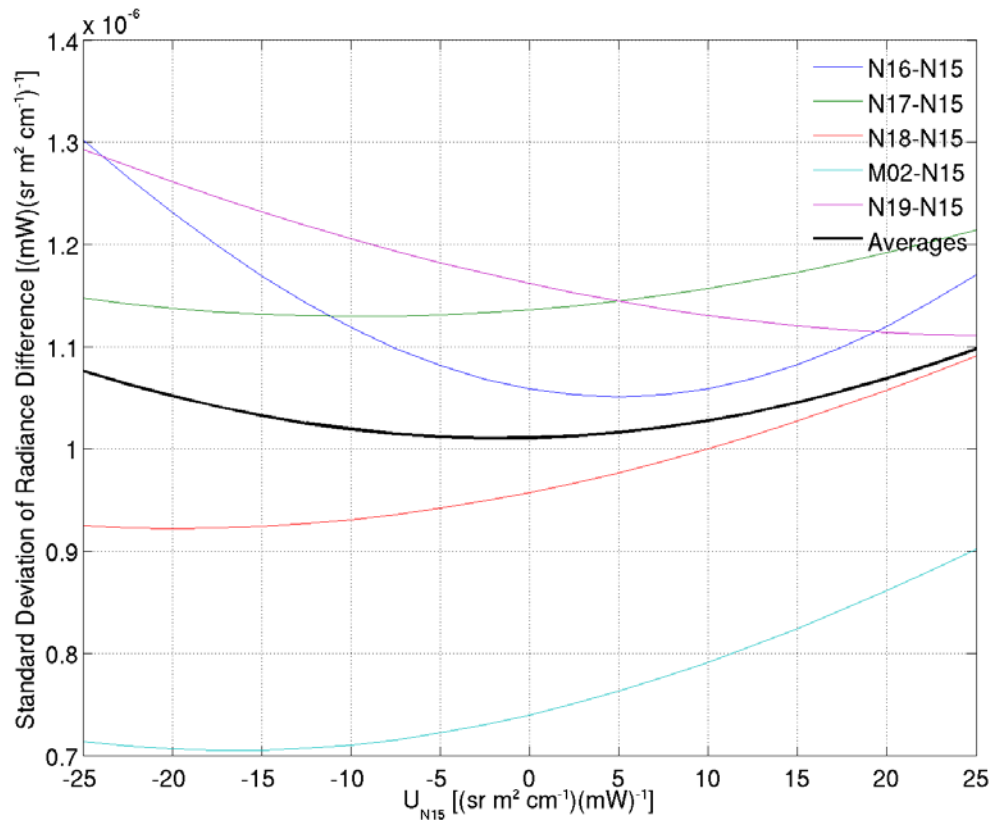


Figure 5: Iterative search for μ_{N15} of 23.8 GHz channel.

After the iterative process, the optimal μ and δR are derived and listed in Table 3. Also given in the table is coefficient κ which is required to correct for bias drift. It is noted that inter-calibrated μ is generally very different from the prelaunch μ .

The optimal μ and δR are applied to calculate the inter-calibrated brightness temperatures for all satellites and years. Figures 6 and 7 compare the time series of the 15-day mean nadir Tb over the tropical ocean before and after inter-calibration correction

Table 3: Optimal μ , δR , and κ

	N15	N16	N17	N18	M02	N19
μ Ch1	-2.90860	-7.75889	-10.30357	0.54319	-3.12837	0.09178

	Ch2	1.05310	-2.15364	-3.06236	3.79401	-4.42838	-0.79372
	Ch3	-1.98488	-2.46439	-1.69333	-1.77138	-3.13583	-1.12520
	Ch15	-3.98007	-6.70802	-6.35800	-5.85813	-6.16404	-5.65483
δR	Ch1	0.000E+00	-4.505E-07	-7.846E-07	1.389E-06	-6.149E-07	-4.975E-07
	Ch2	0.000E+00	1.064E-07	6.151E-08	2.861E-07	-1.104E-07	3.753E-07
	Ch3	0.000E+00	-1.311E-06	-2.104E-06	9.705E-06	-5.078E-06	-4.291E-06
	Ch15	0.000E+00	1.191E-05	-1.983E-06	-4.071E-05	-1.029E-04	-5.833E-05
κ	Ch1	0	0	0	0	0	0
	Ch2	0	0	0	0	0	0
	Ch3	0	1.448E-06	0	0	0	0
	Ch15	0	0	0	0	0	0

Inter-calibration minimizes the impact of warm target contamination. Table 4 compares the STD of ΔT_b calculated from Figure 6(e)-(h) and Figure 7(e)-(h). There is significant reduction in the ΔT_b STD from all satellite pairs shown in the table. The improvements on all channels are approximately 50%. A special issue is an uptrend in the NOAA-16 50.3 GHz measurements. This trend is due to bias drift and has been carefully removed as part of the inter-calibration correction. Another issue encountered is the 89.0 GHz of NOAA-15 which appears to suffer from frequency shift. This problem requires further investigation in future study.

3.4.1.3 Scan Bias Correction

The scan bias in AMSU-A window channels is characterized by taking the difference between the observed and the simulated T_b s over low and mid-latitude oceans (60°S-60°N) under clear sky. The difference is adjusted across scan line by its nadir value so there is no systematic difference at nadir. The bias is asymmetric relative to the nadir, and there is little difference in the asymmetry between ascending and descending nodes. The asymmetry pattern is stable throughout the years examined, but varies noticeably for different satellites. The asymmetry appears to be a result of sensor errors especially polarization related issues. By utilizing the vicarious cold reference (VCR) method and stratifying at the most probable value (MPV) level, the cross-scan asymmetry of AMSU-A window channels characterized by these approaches is illustrated in Figure 8. A third method, vicarious hot reference (VHR), was also adopted to characterize cross-scan

asymmetry in the Amazon region (Figure 9). It provides a reference bias point over radiometrically warm land.

Two approaches are used to correct cross-scan bias: one is based on the characterization of the bias at cold end (Figure 8) and warm end (Figure 9), i.e., two-point correction; and the other uses three-point correction by adding the bias at MPV. The corrected Tbs are shown in Figure 10 for the four AMSU-A channels. Little residual bias is observed for all observations and the individual reference points, i.e. MPV, VCR, and VHR (not shown).

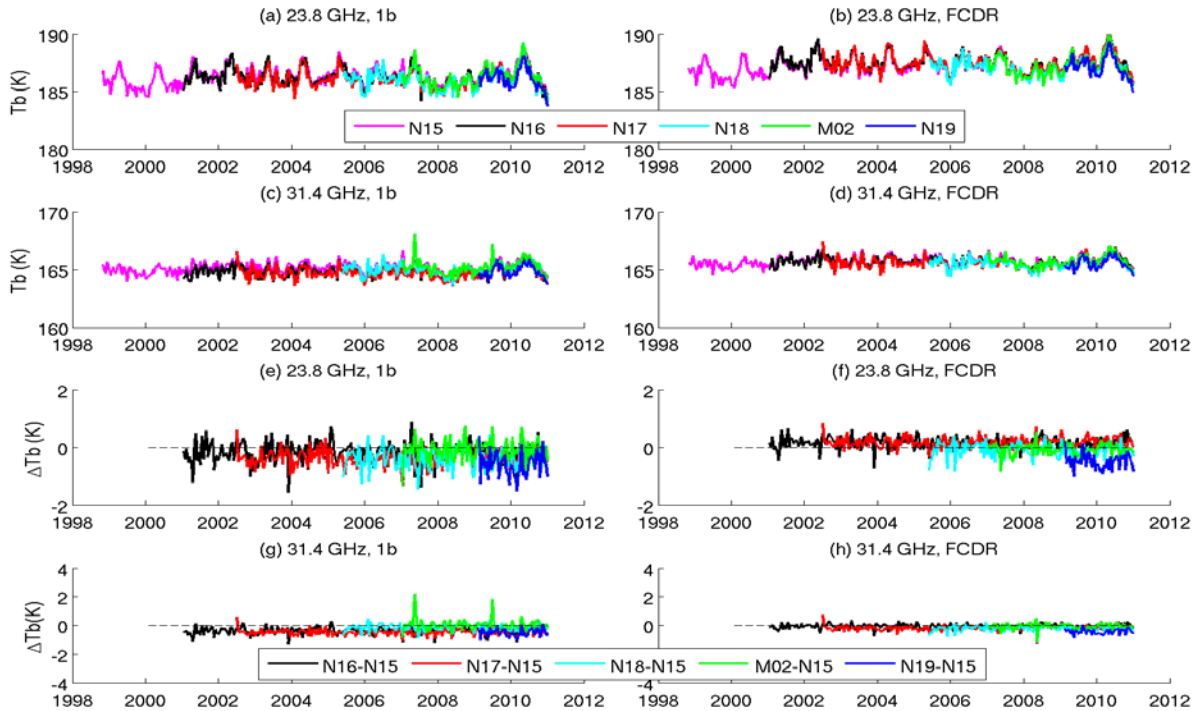


Figure 6: Tropical ocean 15-day mean Tb and ΔT_b for 23.8 and 30.4 GHz channels. Left and right panels are respectively for before and after inter-calibration correction.

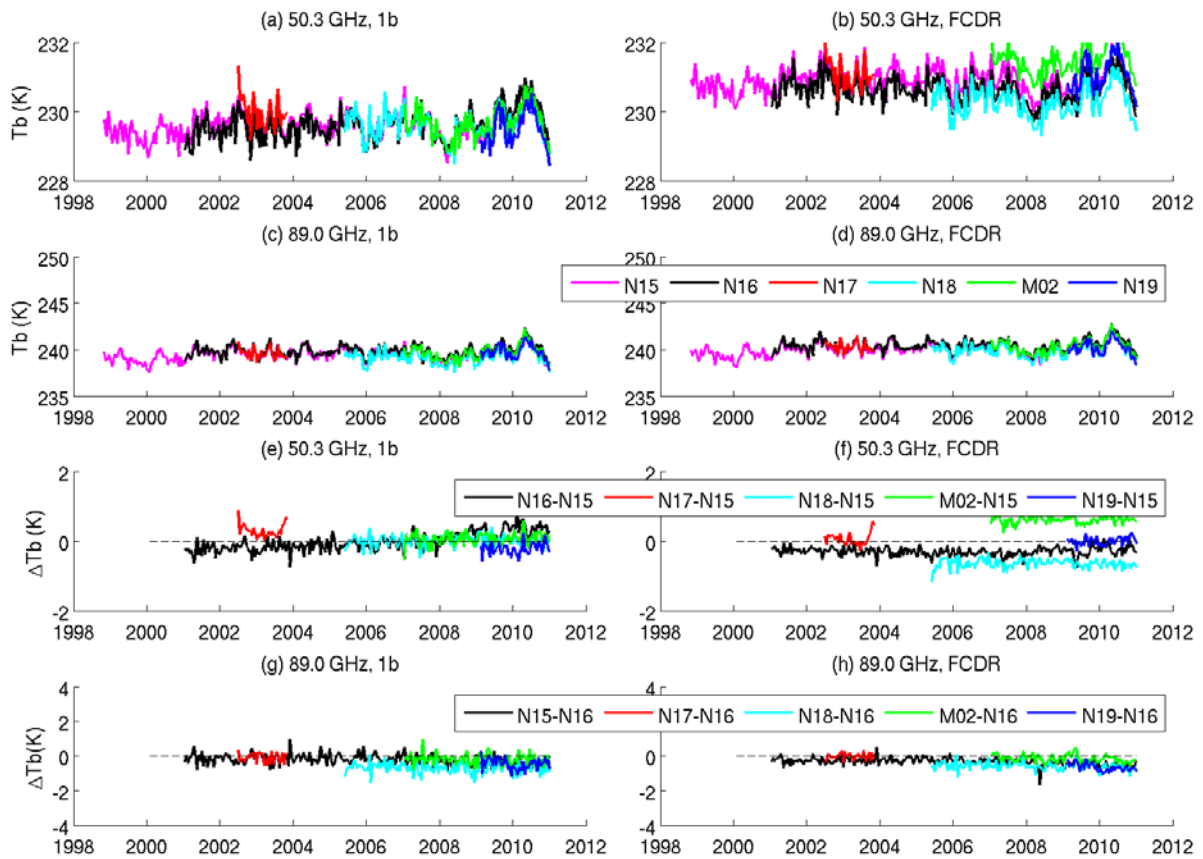


Figure 7: Tropical ocean mean Tb and ΔT_b for 50.3 and 89.0 GHz channels. Left and right panels are respectively for before and after inter-calibration correction.

Table 4: Standard Deviation of ΔT_b over Tropical Ocean

	Before				After			
Channel	23.8	31.4	50.3	89	23.8	31.4	50.3	89
N16-N15	0.374	0.263	0.267	0.315	0.217	0.193	0.126	0.227
N17-N15	0.285	0.217	0.191	0.225	0.191	0.190	0.171	0.132
N18-N15	0.386	0.259	0.168	0.337	0.239	0.197	0.130	0.242
M02-N15	0.37	0.384	0.167	0.328	0.215	0.207	0.108	0.227
N19-N15	0.424	0.276	0.174	0.374	0.263	0.187	0.115	0.208

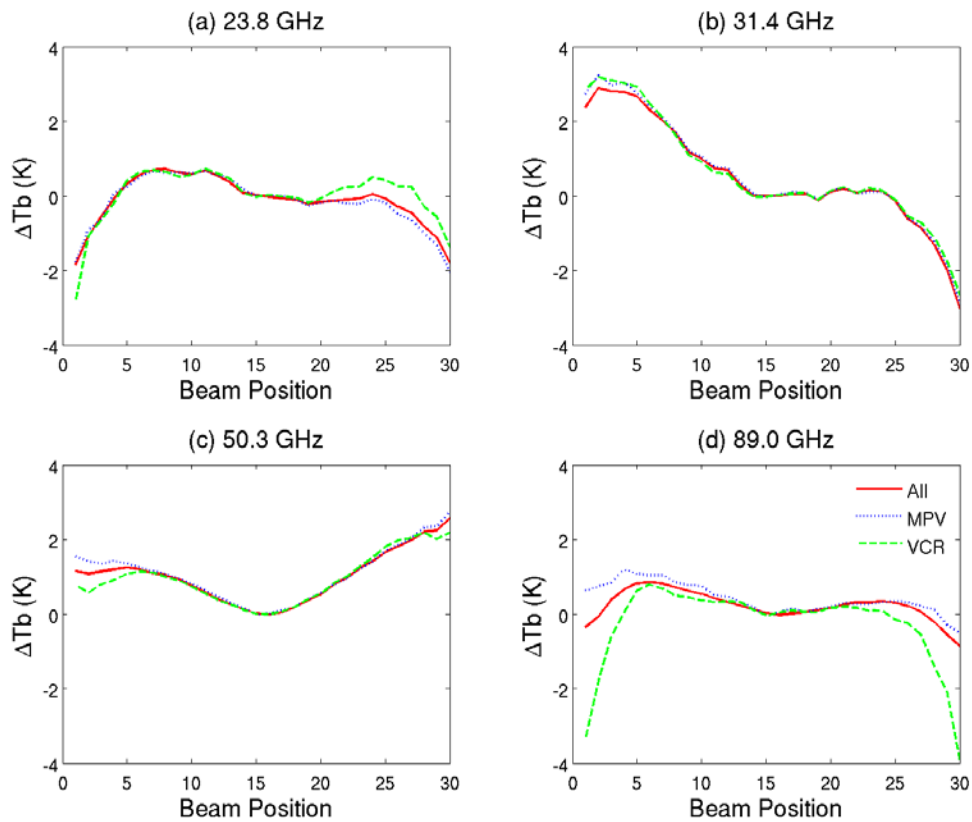


Figure 8: Mean difference between the simulated and the observed NOAA-15 AMSU-A brightness temperatures under clear-sky over ocean in mid- and low-latitude, (a) 23.8, (b) 31.4, (c) 50.3 and (d) 89 GHz. Results are for all observation (All), most probable value stratification (MPV), and vicarious cold reference (VCR). The mean bias is relative to nadir.

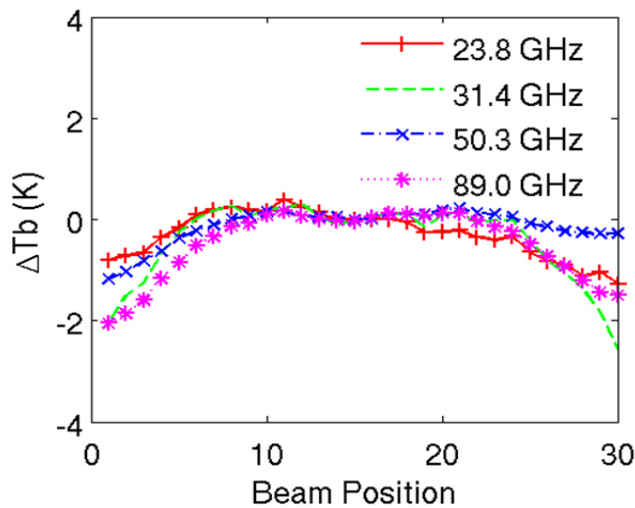


Figure 9: Mean difference between simulated and observed NOAA-15 AMSU-A brightness temperatures at 23.8, 31.4, 50.3 and 89 GHz over Amazon and under clear sky.

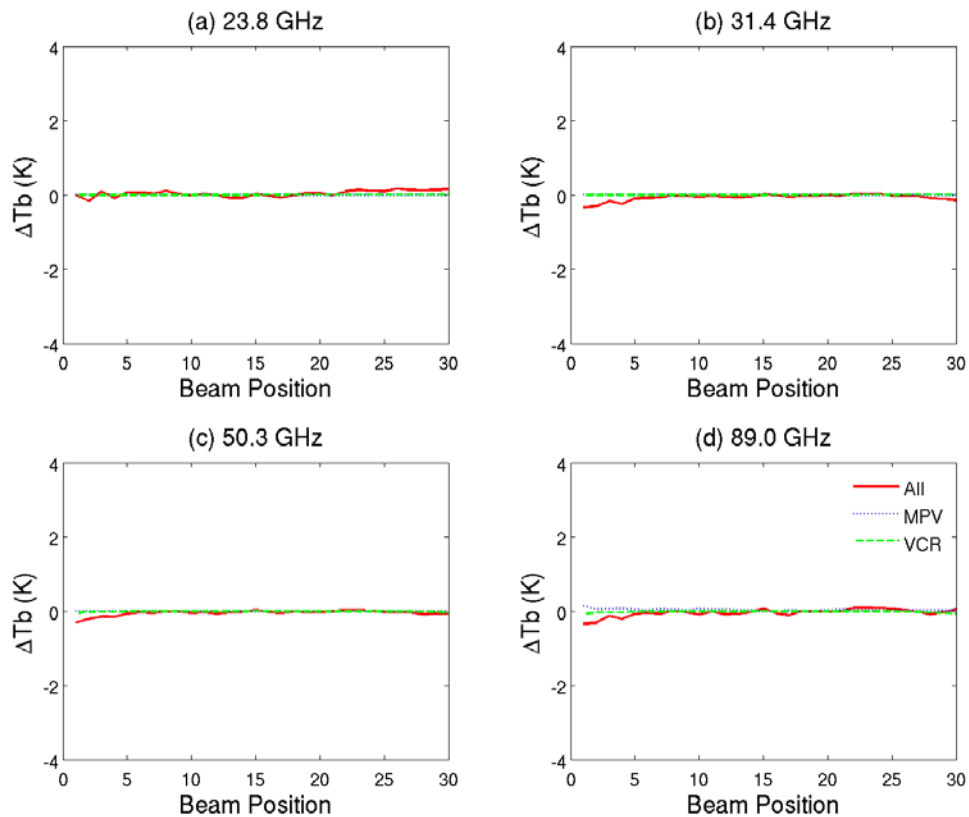


Figure 10: Similar to Figure 8, after the three-point bias correction.

Detailed descriptions of the scan bias correction algorithm, results, and discussions have been published in Yang et al. (2013).

3.4.2 Data Merging Strategy

The original sampling provided by the six AMSU-A sensors is preserved in the output FCDR data with no merging of the resulting data either in space or in time. The resulting T_b FCDR from each of the six sensors are intercalibrated to be physically consistent with the observed T_b from NOAA-15. Asymmetric scan bias has been corrected for each sensor, but the T_b difference due to variations in the view angle or EIA still remain. AMSU-A window channels are subject to the influence from both the atmosphere and the surface, and consequently show diurnal cycle effect especially over land. Since the six satellites have different Equatorial Crossing Time (ECT), i.e. they overpass a certain location on earth at different times of the day, the observations of the AMSU-A window channels from these satellites cannot be merged without removing the diurnal effect in the measurements. Most of the TCDR derived from the AMSU-A FCDR also have diurnal cycle, so it is important for the FCDR to retain its temporal signature so as to preserve the diurnal

properties of the TCDR. Therefore, there is no plan to merge either the FCDR or TCDR for this project.

3.4.3 Numerical Strategy

For geolocation correction, the subroutines to compute the spacecraft position and velocity from the Two-Line Element (TLE) files were implemented based on the North American Aerospace Defense Command (NORAD) SGP code (Vallado et al., 2006). Details on the numerical calculations of the pixel geolocation and associated angles are provided in Moradi et al. (2013).

3.4.4 Calculations

Details on the processing steps involved in the algorithm are provided in Section 3.2.

3.4.5 Look-Up Table Description

Five stages of the algorithm use data that has been calculated and is stored in static look-up tables. The look-up tables used in each stage are described in this section.

3.4.5.1 Inter-Satellite Calibration Coefficients

The Inter-satellite calibration for AMSU-A has been described in Section 3.4.1.2. Look-up table, `mu_dr_k.dat`, as shown in Table 3, stores the optimal μ , δR and k for the four AMSU-A window channels from all satellites. There are 6 columns in the file, each for one satellite, namely NOAA-15, NOAA-16, NOAA-17, NOAA-18, Metop-A, and NOAA-19. There are altogether 12 rows, with the first 4 for μ , the middle 4 for δR , and the last 4 for k . Each four rows are for the four window channels, respectively. Note that NOAA-15 is selected as the reference satellite for channels 1-3, and NOAA-16 for channel 15. No inter-satellite calibration is performed for channel 15 of NOAA-15 due to frequency shift.

3.4.5.2 T_a to T_b Conversion

The antenna pattern correction (APC) coefficients used to convert antenna temperature (T_a) to T_b for AMSU-A are stored in text files `*_APC.dat`, with `*` stands for satellite name, e.g. `N15_APC.dat`. The derivation of these coefficients is described in Mo (1999). The coefficients were provided by Mo (personal communication). Only the APC coefficients for the four AMSU-A window channels are included in the look-up tables.

3.4.5.3 Scan Bias Correction

The scan bias correction coefficients are stored in text files `*_ASYM.dat`, with `*` stands for satellite name, e.g. `N15_ASYM.dat`. The derivation of these coefficients is described in Section 3.4.1.3 and Yang et al. (2013). There are 30 rows in each file, with each row for each beam position. In each row, the first column is the nominal earth incidence angle for the beam position, with beam positions 1-15 assigned negative values, and beam positions 16-30 positive ones. Rows 2-13 are quadratic coefficients for the four window

channels, with Rows 1-5 as a_2 , Rows 6-9 as a_1 , and Rows 10-13 as a_0 in the following correction equation:

$$\Delta Tb = a_2 Tb_o^2 + a_1 Tb_o + a_0 \quad (3-8)$$

where Tb_o is the observed brightness temperature.

3.4.5.4 Latbox Calculation

In order to process microwave sensor observation, it is often important to know the underlying surface type by using a land-sea mask. The land-sea mask included in the AMSU-A FCDR Production Package is a gridded map with cylindrical projection. Since AMSU-A footprint size varies across the scan line due to the cross-scan design, the number of land-sea map pixels falling into each footprint is not fixed even at the same latitude. The look-up table, `latbox_table.dat`, provides the information on how many pixels a footprint should cover based on its beam position.

3.4.5.5 Climatological Quality Check

The lower and upper limits of observed brightness temperatures for the four AMSU-A window channels have been specified in the look-up table `input.dat` based on climatology. If a brightness temperature fails to pass the climatological quality check, a fill value is given, and a flag is set in the corresponding QC bit.

3.4.6 Parameterization

The antenna pattern correction or APC is a parameterization of the measured antenna pattern. It is described in Section 3.3 and by Mo (1999).

3.4.7 Algorithm Output

For each input L1B file, the algorithm produces an output FCDR file in NetCDF4 format. There are approximately 14 files per sensor per day and each file is approximately 840 Kbytes. The FCDR file contains the final intercalibrated Tb for each channel along with Field-Of-View (FOV) latitude and longitude, time for each scan, spacecraft direction, quality flags, solar zenith angle, and earth incidence angle with the necessary metadata and supplementary data fields. Two groups of variables are provided. One group corresponds to the geolocation and time, and the other to the other variables. The data are truncated to the nearest 0.001 degree for the latitude and longitude values and to the nearest 0.01 K for the Tb and 0.01 degree for view angles. Internal NetCDF data compression is used to compress the files. An example of the format of the FCDR files is provided in Appendix C.

4. Test Datasets and Outputs

4.1 Test Input Datasets

The test dataset is composed of one month of AMSU-A four window channels (23.8, 31.4, 50.3, and 89 GHz) Level-1B data from NOAA-15, -16, -17 (only two channels), -18, -19 and Metop-A for September 2009 and the following ancillary data: corrected geolocation data, inter-satellite calibration correction coefficients, scan bias correction coefficients, and land-sea mask data. The corrected geolocation data include latitude, longitude, EIA, and scan angle for each channel. They were generated offline using a geolocation correction approach developed in this project (Moradi et al., 2013). The inter-satellite calibration method developed by Zou et al. (2006, 2009, 2010, and 2011) and the scan bias correction method developed in this study (Yang et al., 2013) were applied to derive the bias correction coefficients. All test input data are operational data. It is noted that, since many of the correction coefficients were derived from long term data, the statistics from the one-month test data will not closely resemble the general statistics of the FCDR dataset.

4.2 Test Output Analysis

4.2.1 Reproducibility

A set of brightness temperature FCDRs derived from the test L1B data during development is also delivered with the test input data. The brightness temperatures generated from the AMSU FCDR processing system using the test input data should reproduce the same FCDRs as the data created during development. Comparisons of basic statistics such as monthly mean and standard deviation of the brightness temperatures between the two data sets will suffice to confirm the reproducibility of the test data.

4.2.2 Precision and Accuracy

This project includes two major accomplishments: inter-satellite calibration and scan bias correction. Precision of the inter-satellite calibrated data is measured by the standard deviation of the brightness temperatures difference between satellite pairs (Table 5). NOAA-15 AMSU-A acts as the reference satellite for channels 1-3 (23.8, 31.4, and 50.3 GHz). NOAA-16 is used as reference for channel 15 (89 GHz) because NOAA-15 channel 15 appears to suffer from frequency shift.

The precision of the cross scan bias is characterized by an Asymmetry Index which is defined as:

$$AI = \sqrt{\frac{\sum_{i=1}^N A_i}{N}} \quad (4-1)$$

$$A_i = \Delta TB_i - \frac{\Delta TB_{15} + \Delta TB_{16}}{2} \quad (4-2)$$

where N is the number of beam positions or field of views in each scan line. For AMSU-A, $N = 30$. ΔTB_i is the difference (bias) between the observed and the simulated reference brightness temperatures at beam position i . The second term in the definition of A_i is the bias at nadir. AI essentially measures the bias relative to nadir for a single satellite. Table 6 gives the AI for the AMSU-A window channels from all satellites.

Table 5: ΔT_b (K) of Brightness Temperature Difference between Satellite Pairs

Frequency (GHz)	23.8	31.4	50.3	89.0
N16-N15	0.217	0.193	0.126	0.227
N17-N15	0.191	0.190	0.171	0.132
N18-N15	0.239	0.197	0.130	0.242
M02-N15	0.215	0.207	0.108	0.227
N19-N15	0.263	0.187	0.115	0.208

Table 6: Asymmetry Index (K) of AMSU-A Window Channels

Channel (GHz)	NOAA-15	NOAA-16	NOAA-17	NOAA-18	Metop-A	NOAA-19
23.8	0.05	0.09	0.20	0.05	0.06	0.11
31.4	0.10	0.03	0.11	0.04	0.05	0.12
50.3	0.21	0.06	0.10	0.08	0.16	0.14
89.0	0.57	0.37	0.48	0.51	0.50	0.56

To determine the accuracy of the FCDR, SI traceable standards for the AMSU-A microwave frequencies are required. However, such standards are not yet available. Also unavailable are reliable and stable vicarious targets that can be used to determine the accuracy of the AMSU-A window channels measurements. The lack of “truth” makes it difficult to compute the accuracy of the AMSU-A FCDR.

4.2.3 Error Budget

The various errors associated with the AMSU-A window channels FCDR data are listed in Table 7. It is noted that these errors cannot be combined in simple forms.

Table 7: Error Budget of AMSU-A Window Channels FCDR

Error Sources	Magnitude of Errors	Prospective Improvements
<i>Inter-satellite calibration</i>	<i>0.1 - 0.3 K for the four channels</i>	<i>Add land training data</i>
<i>Cross scan bias</i>	<i>< 0.2 K for Channel-1 to -3, 0.5 K for Channel 15*</i>	<i>Line by line RTM simulations and more advanced input data</i>
<i>CRTM model uncertainty</i>	<i>2.6 – 3.9 K for the four channels**</i>	<i>Replace CRTM with line by line RTM</i>
<i>ERA-interim data bias</i>	<i>< 1 K ***</i>	<i>Replace ERA-interim with more advanced input data</i>
<i>Geolocation</i>	<i>Most satellites/channels < 10 km, NOAA-15 channel-1 and -2 up to 20 km</i>	<i>Improve yaw correction by using data from limbs</i>

* Based on Asymmetry Index calculation

** Based on Chen et al. (2008)

*** Based on the comparison between ERA-Interim and GDAS (not included)

5. Practical Considerations

5.1 Numerical Computation Considerations

Endian

The AMSU-A FCDR Production Package assumes IEEE little-endian environment. Note the original AMSU L1B data is in IEEE big-endian, so endian swapping is required before further processing.

Precision

The code can be run under either 32-bit or 64-bit mode.

Parallelization

This production package is not considered computationally intensive so parallel computation is not performed.

5.2 Programming and Procedural Considerations

The code that implements the FCDR algorithms follows standard procedural programming constructs. No unusual programming techniques or optimizations are used as simplicity was an important design criterion.

5.3 Quality Assessment and Diagnostics

The output of geo-location correction and scan bias correction has been assessed, and the results are described in Moradi et al. (2013) and Yang et al. (2013). Further assessment of the inter-satellite calibration will be implemented.

5.4 Exception Handling

Error and exception conditions are handled by direct checking of conditions/return codes in the main control flow rather than by a language-supported exception construct.

5.4.1 Conditions Checked

The following conditions identify errors that necessitate the program terminate. These errors are trapped and the program prints a suitable message, then exits gracefully with a non-zero status indicating the type of error.

- If an incorrect number of arguments are supplied to the program, a usage message is printed and it exits.
- If there is an error opening or reading an input file, the program prints an error message and exits.

- If there is an error creating or writing to an output file, the program prints an error message and exits.

The following exceptions are trapped and recovered from by skipping over the item that can't be processed, setting codes to track this, and continuing processing with the next item:

- If there is an error opening or reading a standalone geolocation file, the processing of this orbit is skipped over, and the program execution continues.
- If an orbit has scan number smaller than an allowed limit, the processing of this orbit is skipped over, and the program execution continues.

5.4.2 Conditions Not Checked

The following possible error condition is not checked for:

- In the unlikely event that the program would run out of memory, the process would terminate unexpectedly.

5.4.3 Conditions Not Considered Exceptions

Where data fields are missing or do not satisfy quality control checks (described in Section 3.2.7), quality flags are set, and for those quality issues classified as serious the corresponding data fields are set to indicate missing data. All corrections/conversions are applied only to non-missing data, and if any processing stage identifies certain data as missing, it remains missing for all future processing stages. This is considered normal processing and not an exception condition.

5.5 Algorithm Validation

The algorithm validation has been carried out with regards to geolocation correction, scan bias correction and inter-satellite calibration. Most of the results have been presented in conferences and documented in published papers (Yang, et al., 2013; Moradi, et al., 2013). Below is a summary of the studies. Effort on validating the inter-satellite calibration is still on going.

5.5.1 Geolocation Correction

Our study shows that NOAA-15 AMSU-A2 (channels 1 and 2) has the largest geolocation error. Figure 11 shows that this unit is mounted about 1.2 degrees negative cross track, so that the instrument does not point to the satellite subpoint when the scan angle is zero. Other problems that we found in the level L1B data are as follows:

- The clock offset correction for NOAA-17 AMSU-A sensor has been turned off. The clock offset has a large impact on geolocation accuracy that 1 second clock offset is roughly equal to 6 km along track geolocation error.

- NOAA-15 clock offset was not included in level L1B geolocation from satellite launch in 1998 to early 2001. This offset was sometimes more than 2 seconds and could shift data by about 12 km along track.
- The L1B geolocation package failed to calculate Greenwich Hour Angle (GHA) for about 10 days at the beginning of 2004. Those data have a very large geolocation error with about 1-degree offset in longitude.
- L1B geolocation data were in geocentric coordinates instead of geodetic coordinates before year 2007.

All the errors mentioned above have been corrected in this project. Figure 12 compares the ΔT_b before and after geolocation correction for NOAA-15 AMSU-A 23.8 GHz.

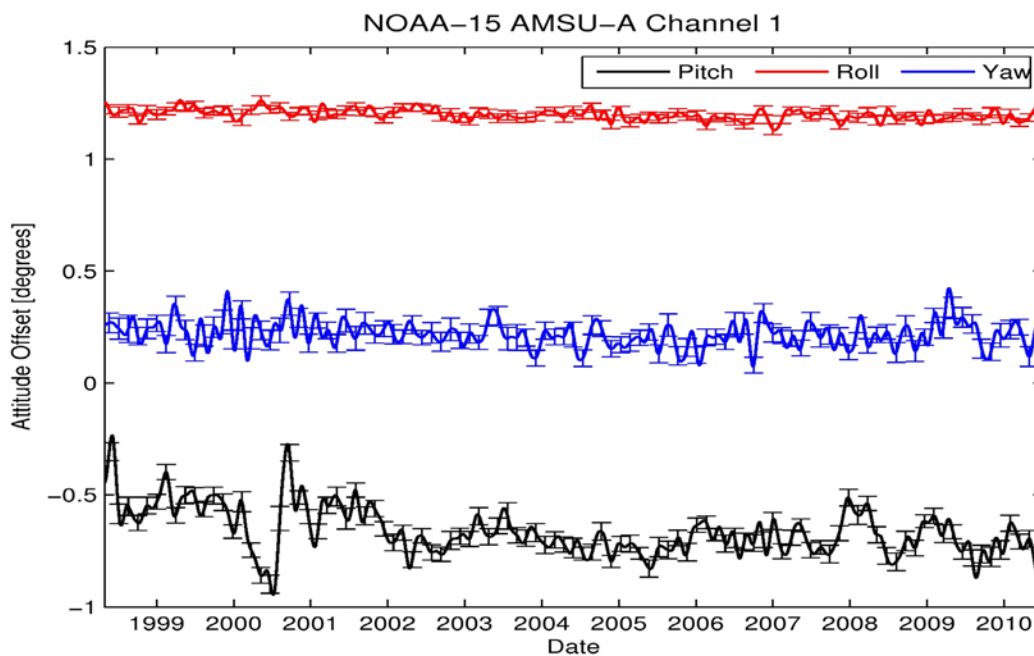


Figure 11: Time series of the satellite attitudes for NOAA-15 AMSU-A 23.8 GHz (channel 1). AMSU-A2 instrument is mounted about 1.2 degrees negative cross-track, so the sensor does not point to the nadir when the scan angle is zero. The sensor has a small along track offset as well, about 0.5 degree.

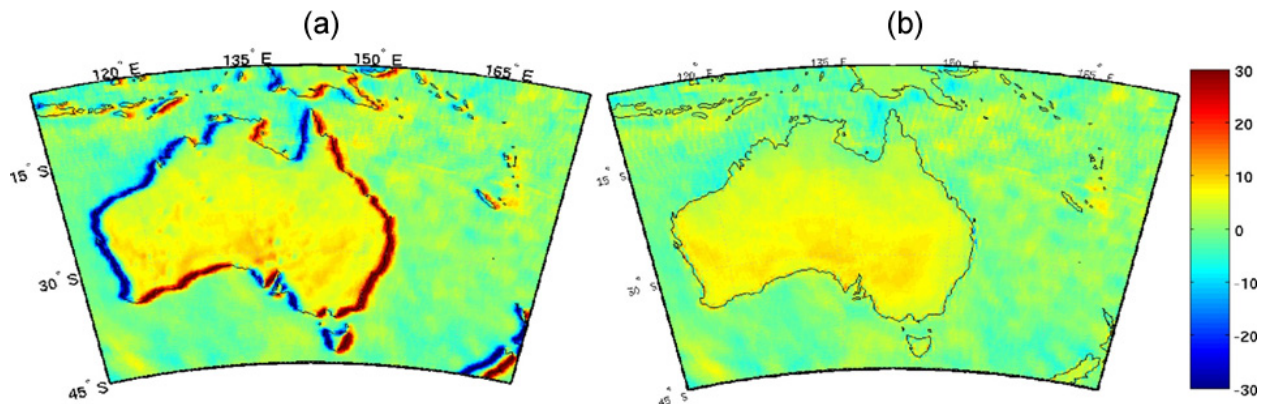


Figure 12: Difference between ascending and descending brightness temperatures from NOAA-15 AMSU-A 23.8 GHz channel, (a) before correction; (b) after correction.

5.5.2 Scan Bias Correction

The validation of scan bias correction has been performed on both FCDR and TCDR. The FCDR results have been shown in Section 3.4.1.3, especially Figure 10.

With TCDR, the improvement is evident in the products when the scan bias correction is applied. Figure 13 compares two Level-2 (L2) products, cloud liquid water (CLW) and emissivity at 31.4 GHz, before and after the scan bias correction. Before correction, the scan bias effect is clearly seen in the CLW image (Figure 13a) with drier atmosphere at the left edge of the swath and wetter at the opposite edge, which makes the cloud system unrealistic. For instance, compared to the uncorrected CLW image, the corrected version has a much more coherent cloud structure above the vast ocean area at mid- and high-latitudes of Southern Hemisphere (Figure 13b). The corrected 31.4 GHz emissivity (Figure 13d) also exhibits much improvement in its cross-scan symmetry than the original (Figure 13c). This is most noticeable in the 15°N to about 37°N latitude bands where the lower emissivity is asymmetric at the two limbs in the original image but becomes comparable after correction. In summary, scan bias correction makes the angular distribution much more symmetric and realistic. It is worth noting that the CDR scan bias cross-scan approach outperforms the current operational correction approach used in MSPPS, which is essentially a one-point correction. The significant reduction in scan bias in the CDR products shows that the bias correction scheme for AMSU-A window channels is effective.

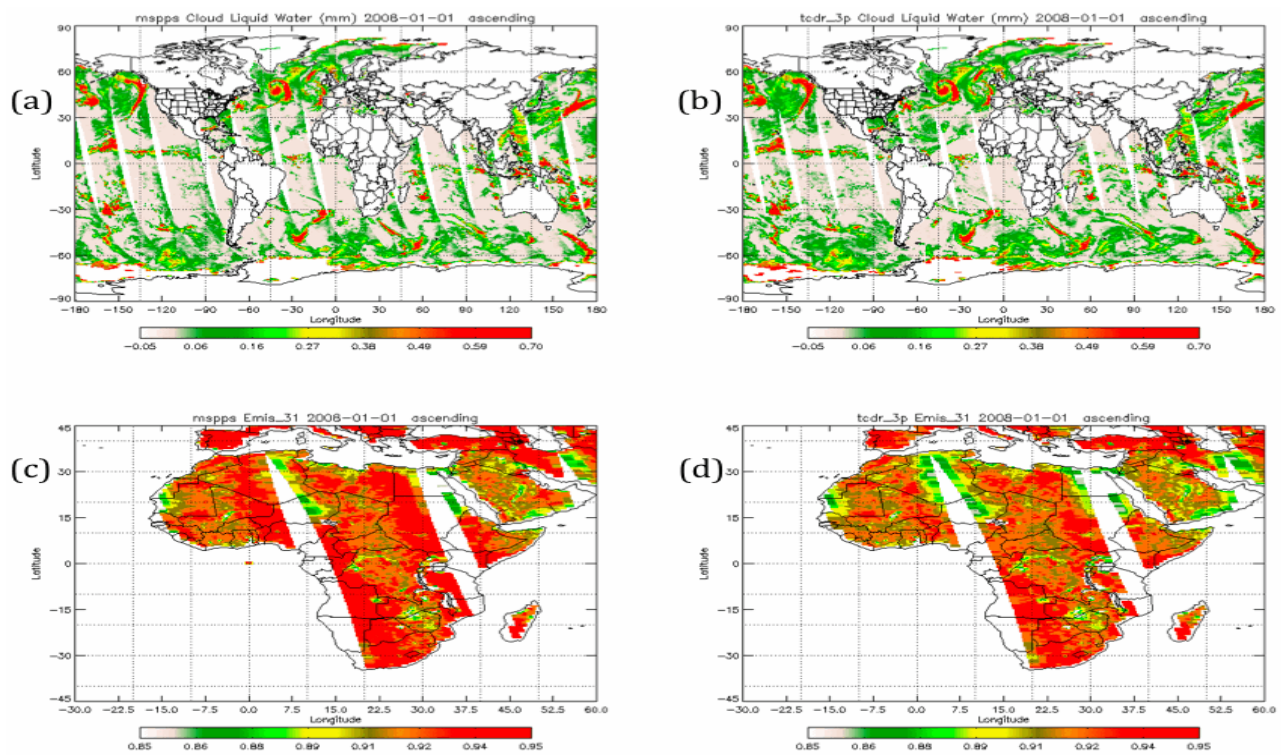


Figure 13: Geographical distribution of cloud liquid water (upper panels) and land surface emissivity at 31.4 GHz (lower panels), derived through MSPPS. Images (a) and (c) are the original products; and (b) and (d) are with scan bias correction. For clarity, the 31.4 GHz emissivity is shown over the continent of Africa instead of the entire globe.

5.5.3 Inter-Satellite Calibration

For Inter-Satellite Calibration, the overall validation results have been given in Section 3.4.1.2, especially Figure 6, 7, and Table 4.

Two sets of additional validation studies have been planned to further examine the effectiveness of the inter-satellite calibration. In the first study, the geographical distribution of radiance before and after inter-satellite calibration will be compared, especially in later years. Similar to the validation of scan bias correction, the inspection of adequate inter-satellite calibration will also be extended to geophysical retrievals, i.e. TCDR. Time series of selected variables before and after inter-satellite calibration will be compared for consistency.

5.6 Processing Environment and Resources

Computer Hardware: Linux x86_64, 132 GB memory
 Operating System: Red Hat Enterprise Linux Server release 6.5 (Santiago)
 Programming Language: C
 Compilers: gcc 4.4.7-4
 External Libraries: NetCDF 4.1.1
 Total CPU Time: about 21m per satellite year
 Wall Clock Time: about 53m per satellite year
 Temporary Storage: 4.3 GB per satellite year.

6. Assumptions and Limitations

6.1 Algorithm Performance

The inter-satellite calibration is performed following the approach developed by Zou et al. (2006, 2009, 2010, and 2011). This method is extremely sensitive to the quality of the input data. Special caution has been taken in this study to filter input data such as setting strict threshold for brightness temperature difference when choosing SNO data.

The cross scan bias correction heavily relies on the brightness temperatures simulated using the Community Radiative Transfer Model (CRTM). In addition, ERA-interim reanalysis data are used as the input for CRTM. Both the uncertainties in CRTM simulation and in ERA-interim data could potentially degrade the effectiveness of the cross scan bias correction method. It is desired to improve scan bias correction in the future with a line by line radiative transfer model and more advanced reanalysis data.

6.2 Sensor Performance

Several sensor issues were noticed during the course of this project. First, NOAA-16 channel 3 (50.3 GHz) is found to have significant bias drift. This drift is corrected by adding a third term, κ , in the inter-satellite calibration correction equation (Zou et al., 2011). The time series of NOAA-16 channel 3 brightness temperature before and after de-trending is displayed in Figure 14.

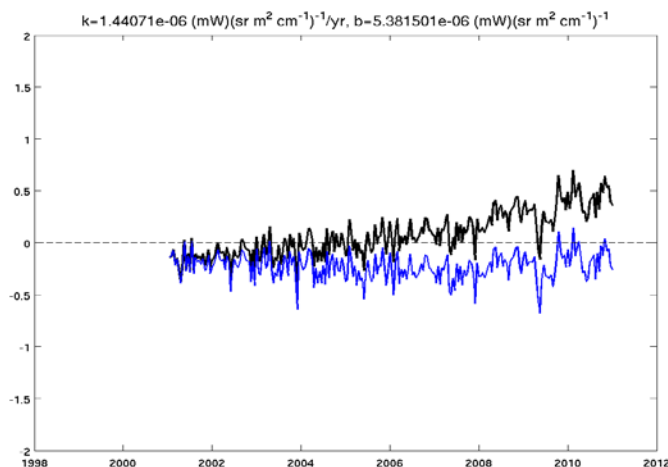


Figure 14: Time series of NOAA-16 channel 3 brightness temperature before (black) and after (blue) de-trending

The second issue related to sensor is with NOAA-15 AMSU-A2 unit. Geolocation study results reveal a mounting error of about 1.2° cross-track and -0.5° along-track for this instrument. The effects of the mounting error have been removed with a geolocation correction approach developed in this project (Moradi et al, 2013).

Finally, NOAA-15 channel 15 is discovered to suffer from frequency shift after many failed inter-satellite calibrations for this channel. However, this issue is not resolved in this project due to time constraint.

7. Future Enhancements

7.1 Enhancement 1 – Extension of NOAA-15 FCDR Record

NOAA-15 was launched on May 13, 1998 while the current NOAA-15 AMSU-A FCDR starts on January 1, 2000. With some additional effort, the NOAA-15 FCDR record can be extended back to late October 1998.

7.2 Enhancement 2 – Correction of Frequency Shift

It was discovered in this project that NOAA-15 channel-15 (89 GHz) appears to suffer from frequency shift. This issue was not solved in the current project due to time constraint. However, it is possible to correct the frequency shift problem with the aid of radiative transfer simulations.

7.3 Enhancement 3 – Inter-Satellite Calibration over Land

The inter-satellite calibration has been performed over tropical ocean to take advantage of the weak diurnal cycle effect and data homogeneity in this region. Since land emissivity is about twice as high as ocean emissivity, the brightness temperature over land is usually much higher than over ocean in tropical and sub-tropical regions. Therefore, the inter-satellite calibration results are more representative of the low end of the brightness temperature range rather than of the higher brightness temperatures. Since inter-satellite bias can be scene temperature dependent, it is desirable that inter-satellite calibration is also performed over land in the future. A significant challenge to overcome in the future study will be to accurately model the diurnal effect in window channels over land.

7.4 Enhancement 4 – Improving Cross Scan Asymmetry Correction

The cross scan asymmetry correction conducted in this study is based on the simulations of CRTM with ERA-Interim reanalysis as input data. Since the simulated brightness temperatures play a critical role in characterizing the cross scan asymmetry in the observations, more accurate simulations will directly improve the cross scan asymmetry and, consequently, the quality of the FCDR. It is recommended that a line by line RTM is used in the future for brightness temperature simulation. It is also advantageous to choose a more advanced reanalysis dataset as input should one become available. A major challenge in using a line by line RTM for CDR will be the overwhelming expense of computer time.

8. References

- Chen, Y., Weng, F., Han, Y., and Liu, Q (2008). Validation of the Community Radiative Transfer Model by using CloudSat data, *J. Geophys. Res.*, vol. 113, D00A03, doi:10.1029/2007JD009561.
- EUMETSAT (2010). *ATOVS Level L1B Product Guide*, available at <http://oiswww.eumetsat.org/WEBOPS/eps-pg/ATOVS-L1/ATOVSL1-PG-index.htm>.
- Ferraro, R.R., F. Weng, N. Grody, L. Zhao, H. Meng, C. Kongoli, P. Pellegrino, S. Qiu and C. Dean (2005). NOAA operational hydrological products derived from the AMSU. *IEEE Trans. Geo. Rem. Sens.*, 43: 1036 – 1049.
- Kidwell, K.B., edited (1998). *NOAA Polar Orbiter Data User's Guide*, available at <http://www.ncdc.noaa.gov/oa/pod-guide/ncdc/docs/podug/index.htm>.
- Mo, T (1999). AMSU-A antenna pattern corrections. *IEEE Trans. Geosci. Remote Sens.*, 37(1): 103-112, 1999.
- Moradi, I., H. Meng, R.R. Ferraro, and S. Bilanow (2013). Correcting geolocation errors for microwave instruments aboard NOAA satellites. *IEEE Trans. Geosci. Remote Sens.*, 51, 3625-3637. DOI: 10.1109/TGRS.2012.2225840.
- Robel, J., *et al.* edited (2009). *NOAA KLM User's Guide*, available at <http://www.ncdc.noaa.gov/oa/pod-guide/ncdc/docs/podug/index.htm>.
- D. A. Vallado, P. Crawford, R. Hujsak, and T. Kelso, Revisiting spacetrack report #3. AIAA/AAS Astrodynamics Specialist Conf., Keystone, CO, American Institute of Aeronautics and Astronautics, Aug. 2006.
- Yang, W., H. Meng, R. Ferraro, I. Moradi, and C. Devaraj (2013). Cross scan asymmetry of AMSU-A window channels: characterization, correction and verification. *IEEE Trans. Geosci. Remote Sens.*, 51, 1514-1530. DOI:10.1109/TGRS.2012.2211884.
- Zou, C.-Z., M. Goldberg, Z. Cheng, N. Grody, J. Sullivan, C. Cao, and D. Tarpley (2006). Recalibration of microwave sounding unit for climate studies using simultaneous nadir overpasses. *J. Geophys. Res.*, 111, D19114, doi:10.1029/2005JD006798.
- Zou, C.-Z., M. Gao, and M. Goldberg (2009). Error structure and atmospheric temperature trends in observations from the Microwave sounding Unit. *J. Clim.*, 22, 1661–1681, doi:10.1175/2008JCLI2233.1.
- Zou, C.-Z., and W. Wang (2010). Stability of the MSU-derived atmospheric temperature trend. *J. Atmos. Oceanic Technol.*, 27, 1960–1971, doi:10.1175/2009JTECHA1333.1.
- Zou, C.-Z., and W. Wang (2011). Intersatellite calibration of AMSU-A observations for weather and climate applications. *J. Geophys. Res.*, 116, D23113, doi:10.1129/2011JD016205.

Appendix A. Acronyms and Abbreviations

Acronym or Abbreviation	Meaning
AMSU	Advanced Microwave Sounding Unit
AMSU-A	Advanced Microwave Sounding Unit-A
AMSU-B	Advanced Microwave Sounding Unit-B
ATMS	Advanced Technology Microwave Sounder
ATOVS	Advanced Tiros Operational Vertical Sounder
C-ATBD	Climate Algorithm Theoretical Basis Document
CDR	Climate Data Record
CICS	Cooperative Institute for Climate and Satellites
ECMWF	European Centre for Medium-Range Weather Forecast
ECT	Equator crossing time
EIA	Earth Incidence Angle
EUMETSAT	European Organization for the Exploitation of Meteorological Satellites
FCDR	Fundamental Climate Data Record
FOV	Field of View
HIRS	High-resolution Infrared Radiation Sounder
IFOV	Instantaneous Field of View
JPSS	Joint Polar Satellite System
LST	Local Standard Time
MetOp	Meteorological Operational Polar Satellite
MHS	Microwave Humidity Sounder
NCDC	National Climatic Data Center
MSPPS	Microwave Surface and Precipitation Products System
NESDIS	National Environmental Satellite, Data, and Information Service
NCEP	National Centers for Environmental Prediction
NeDT	Noise Equivalent Difference of Temperature
NOAA	National Oceanic and Atmospheric Administration
POES	Polar-orbiting Operational Environmental Satellites
RMSE	Root Mean Square Error
SSM/I	Special Sensor Microwave/Imager
STAR	Center for Satellite Applications and Research
TB	Brightness Temperature
TCDR	Thematic Climate Data Record

TIROS	Television Infrared Observation Satellite
TOVS	TIROS Operational Vertical Sounder

Appendix B. AMSU-A Sensor Details

This appendix provides more detailed information on the AMSU-A sensor. This sensor is flown on the following satellites:

Satellite	Launch Date
NOAA-15	5/13/1998
NOAA-16	9/21/2000
NOAA-17	6/24/2002
NOAA-18	5/20/2005
NOAA-19	2/6/2009
MetOp-A	10/19/2006

The AMSU-A is a fifteen-channel microwave radiometer that is used for measuring global atmospheric temperature profiles and providing information on atmospheric water in all of its forms. Sensor details are provided in the table below. Hardware for the two lowest frequencies is located in one module (AMSU-A2) and that for the remaining thirteen frequencies in the second module (AMSU-A1). The AMSU-A2 module has a single antenna assembly, providing data for channels 1 and 2. AMSU-A1 has two separate antenna assemblies: AMSU-A11 provides data for channels 6, 7 and 9-15, and AMSU-A12 provides data for channels 3, 4, 5 and 8.

AMSU-A operates in a cross-track, stepped-line scanning geometry. The instrument has an instantaneous field-of-view of 3.3° at the half-power points providing a nominal spatial resolution at nadir of 48 km (29.8 mi). The antenna provides a cross-track scan, scanning $\pm 48.3^\circ$ from nadir with a total of 30 Earth fields-of-view per scan line. This instrument completes one scan every 8 seconds.

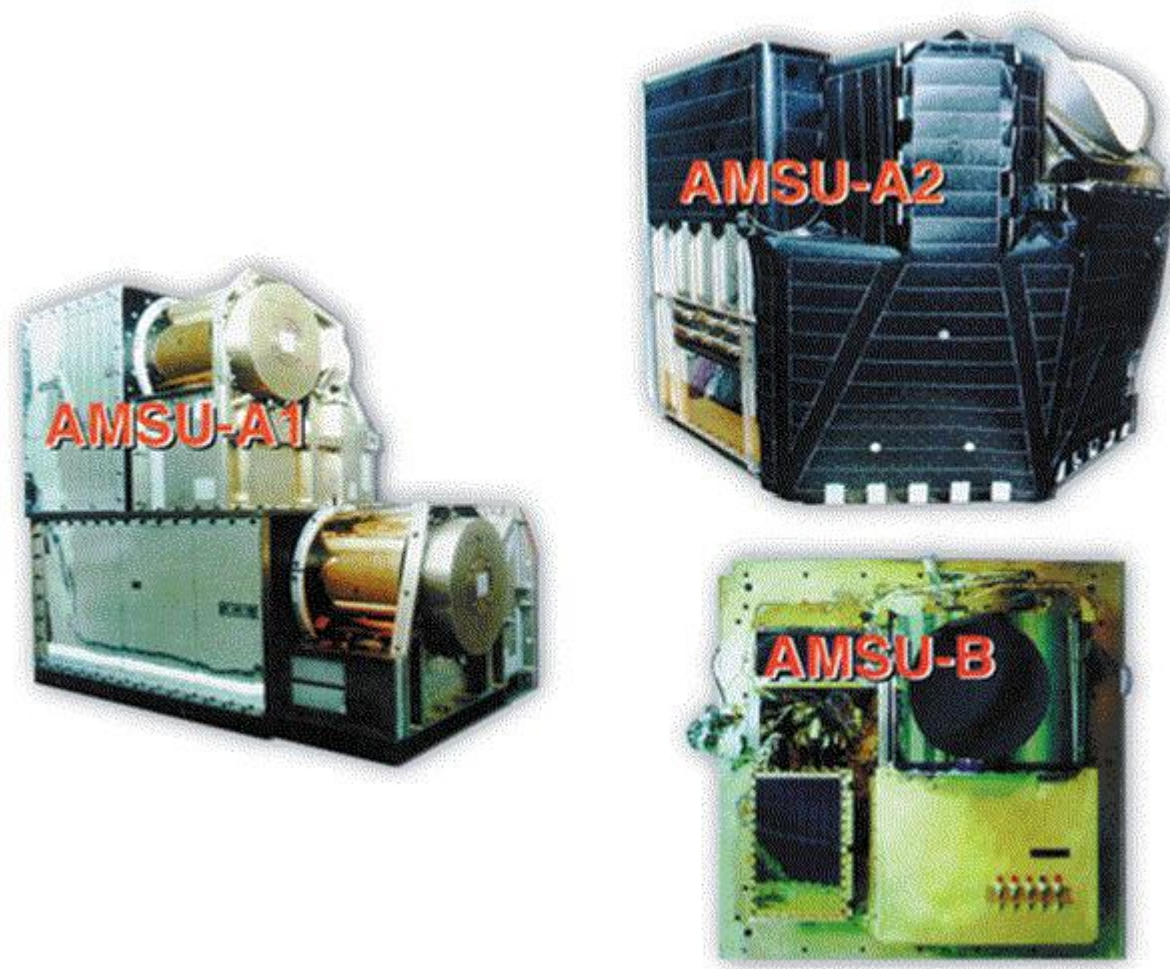
AMSU-A Channel Characteristics

Channel Number	Central Freq. (MHz)	# Bands	Nominal Bandwidth (MHz)	Nominal Beamwidth (degree)	Central Frequency Stability (MHz)	Temperature Sensivity (K) $NE\Delta T$	Calibration Accuracy (K)	Polarization at nadir
1	23800	1	270	3.3	10	0.3	2.0	V
2	31400	1	180	3.3	10	0.3	2.0	V
3	50300	1	180	3.3	10	0.4	1.5	V
4	52800	1	400	3.3	5	0.25	1.5	V
5	53596 ± 115	2	170	3.3	5	0.25	1.5	H
6	54400	1	400	3.3	5	0.25	1.5	H
7	54940	1	400	3.3	5	0.25	1.5	V
8	55500	1	330	3.3	10	0.25	1.5	H
9	57290.344	1	330	3.3	0.5	0.25	1.5	H
10	57290.344 ± 217	2	78	3.3	0.5	0.4	1.5	H
11	57290.344 ± 322.2 ± 48	4	36	3.3	1.2	0.4	1.5	H
12	57290.344 ± 322.2 ± 22	4	16	3.3	1.2	0.6	1.5	H
13	57290.344 ± 322.2 ± 10	4	8	3.3	0.5	0.80	1.5	H
14	57290.344 ± 322.2 ± 4.5	4	3	3.3	0.5	1.20	1.5	H
15	89000	1	<6000	3.3	50	0.5	2.0	V

V: Polarization vector is parallel to scan plane at nadir

H: Polarization vector is perpendicular to scan plane at nadir

AMSU-A



Appendix C. Sample AMSU-A FCDR File Format

```
netcdf CICS_V00R01_AMSUA_FCDR_N15_D10365_S221317_E235909_B6569192 {
dimensions:
    nscan = 795 ;
    npixel = 30 ;
    nchar = 20 ;
    nchan = 4 ;

// global attributes:
    :Conventions = "CF-1.5" ;
    :Metadata_Conventions = "CF-1.5, Unidata Dataset Discovery
v1.0, NOAA CDR v1.0, GDS v2.0" ;
    :standard_name_vocabulary = "CF Standard Name Table (v18, 22
July 2011)" ;
    :id =
"CICS_V00R01_AMSUA_FCDR_N15_D10365_S221317_E235909_B6569192.nc" ;
    :naming_authority = "gov.noaa.ncdc" ;
    :metadata_link = "gov.noaa.ncdc:TBD" ;
    :title = "CICS Version-1 AMSUA FCDR" ;
    :product_version = "v00r02" ;
    :date_issued = "TBD" ;
    :summary = "TBD" ;
    :keywords = "EARTH SCIENCE > SPECTRAL/ENGINEERING >
MICROWAVE > BRIGHTNESS TEMPERATURE" ;
    :keywords_vocabulary = "NASA Global Change Master Directory
(GCMD) Earth Science Keywords, Version 6.0" ;
    :platform = "NOAA-15 > National Oceanic and Atmospheric
Administration - 15" ;
    :sensor = "AMSU-A > Advanced Microwave Sounding Unit - A" ;
    :cdm_data_type = "Swath" ;
    :cdr_program = "NOAA Climate Data Record Program for
satellites, FY 2011" ;
    :cdr_variable = "fcd_r_brightn_ess_t_23,
fcd_r_brightn_ess_t_31, fcd_r_brightn_ess_t_50,
fcd_r_brightn_ess_t_89" ;
    :source = "NSS.AMAX.NK.D10365.S2213.E2359.B6569192.GC" ;
    :references = "TBD" ;
    :history = "TBD" ;
    :date_created = "2013-12-14 07:30:50Z" ;
    :creator_name = "Huan Meng, Ralph R Ferraro" ;
    :creator_url = "http://cics.umd.edu/AMSU-CDR/home.html" ;
    :creator_email = "Huan.Meng@noaa.gov,
Ralph.R.Ferraro@noaa.gov" ;
    :institution = "DOC/NOAA/NESDIS/STAR/CoRP > Cooperative
Research Program, Center for Satellite Applications and Research,
NESDIS, NOAA, U.S. Department of Commerce" ;
    :processing_level = "NOAA level 2" ;
    :geospatial_lat_min = -89.375f ;
    :geospatial_lat_max = 89.411f ;
```

```
:geospatial_lon_min = -179.942f ;
:geospatial_lon_max = 179.938f ;
:geospatial_lat_units = "degrees_north" ;
:geospatial_lon_units = "degrees_east" ;
:spatial_resolution = "48km X 48km at nadir, 150km X 80km at
limb" ;
:time_coverage_start = "2010-12-31 22:13:17Z" ;
:time_coverage_end = "2010-12-31 23:59:09Z" ;
:time_coverage_duration = "P6352S" ;
:license = "No restrictions on access or use" ;
:contributor_name = "TBD" ;
:contributor_role = "TBD" ;

group: Data_Fields {
  variables:
    ubyte orbital_mode(nscan) ;
      orbital_mode:long_name = "satellite direction" ;
      orbital_mode:flag_values = 0UB, 1UB ;
      orbital_mode:flag_meanings = "northbound, southbound" ;
      orbital_mode:_FillValue = 255UB ;
    byte surface_type_a1_1(nscan, npixel) ;
    byte surface_type_a1_2(nscan, npixel) ;
    byte surface_type_a2(nscan, npixel) ;
    float earth_incidence_angle_a1_1(nscan, npixel) ;
      earth_incidence_angle_a1_1:long_name = "earth incidence
angle for AMSU unit A1-1, e.g., 89.0 GHz" ;
      earth_incidence_angle_a1_1:scale_factor = 1.f ;
      earth_incidence_angle_a1_1:_FillValue = -999.f ;
      earth_incidence_angle_a1_1:units = "degree" ;
      earth_incidence_angle_a1_1:coordinates = "latitude_a1_1
longitude_a1_1" ;
    float earth_incidence_angle_a1_2(nscan, npixel) ;
      earth_incidence_angle_a1_2:long_name = "earth incidence
angle for AMSU unit A1-2, e.g., 50.3 GHz" ;
      earth_incidence_angle_a1_2:scale_factor = 1.f ;
      earth_incidence_angle_a1_2:_FillValue = -999.f ;
      earth_incidence_angle_a1_2:units = "degree" ;
      earth_incidence_angle_a1_2:coordinates = "latitude_a1_2
longitude_a1_2" ;
    float earth_incidence_angle_a2(nscan, npixel) ;
      earth_incidence_angle_a2:long_name = "earth incidence
angle for AMSU unit A2, including 23.8 GHz and 31.4 GHz" ;
      earth_incidence_angle_a2:scale_factor = 1.f ;
      earth_incidence_angle_a2:_FillValue = -999.f ;
      earth_incidence_angle_a2:units = "degree" ;
      earth_incidence_angle_a2:coordinates = "latitude_a2
longitude_a2" ;
    float solar_zenith_angle(nscan, npixel) ;
      solar_zenith_angle:standard_name = "solar zenith angle" ;
      solar_zenith_angle:long_name = "solar zenith angle for all
AMSU-A units" ;
```

```
solar_zenith_angle:scale_factor = 1.f ;
solar_zenith_angle:_FillValue = -999.f ;
solar_zenith_angle:units = "degree" ;
float fcdr_brightness_temperature_23(nscan, npixel) ;
fcdr_brightness_temperature_23:standard_name =
"brightness_temperature" ;
fcdr_brightness_temperature_23:long_name = "NOAA FCDR of
23.8 GHz brightness temperature" ;
fcdr_brightness_temperature_23:scale_factor = 1.f ;
fcdr_brightness_temperature_23:lower_limit = 125.f ;
fcdr_brightness_temperature_23:upper_limit = 310.f ;
fcdr_brightness_temperature_23:_FillValue = -999.f ;
fcdr_brightness_temperature_23:units = "kelvin" ;
fcdr_brightness_temperature_23:coordinates = "latitude_a2
longitude_a2" ;
float fcdr_brightness_temperature_31(nscan, npixel) ;
fcdr_brightness_temperature_31:standard_name =
"brightness_temperature" ;
fcdr_brightness_temperature_31:long_name = "NOAA FCDR of
31.4 GHz brightness temperature" ;
fcdr_brightness_temperature_31:scale_factor = 1.f ;
fcdr_brightness_temperature_31:lower_limit = 125.f ;
fcdr_brightness_temperature_31:upper_limit = 310.f ;
fcdr_brightness_temperature_31:_FillValue = -999.f ;
fcdr_brightness_temperature_31:units = "kelvin" ;
fcdr_brightness_temperature_31:coordinates = "latitude_a2
longitude_a2" ;
float fcdr_brightness_temperature_50(nscan, npixel) ;
fcdr_brightness_temperature_50:standard_name =
"brightness_temperature" ;
fcdr_brightness_temperature_50:long_name = "NOAA FCDR of
50.3 GHz brightness temperature" ;
fcdr_brightness_temperature_50:scale_factor = 1.f ;
fcdr_brightness_temperature_50:lower_limit = 150.f ;
fcdr_brightness_temperature_50:upper_limit = 310.f ;
fcdr_brightness_temperature_50:_FillValue = -999.f ;
fcdr_brightness_temperature_50:units = "kelvin" ;
fcdr_brightness_temperature_50:coordinates =
"latitude_a1_2 longitude_a1_2" ;
float fcdr_brightness_temperature_89(nscan, npixel) ;
fcdr_brightness_temperature_89:standard_name =
"brightness_temperature" ;
fcdr_brightness_temperature_89:long_name = "NOAA FCDR of
89.0 GHz brightness temperature" ;
fcdr_brightness_temperature_89:scale_factor = 1.f ;
fcdr_brightness_temperature_89:lower_limit = 130.f ;
fcdr_brightness_temperature_89:upper_limit = 315.f ;
fcdr_brightness_temperature_89:_FillValue = -999.f ;
fcdr_brightness_temperature_89:units = "kelvin" ;
fcdr_brightness_temperature_89:coordinates =
"latitude_a1_1 longitude_a1_1" ;
```

```
    ubyte product_quality_flag(nscan, nchan) ;
        product_quality_flag:long_name = "instrument/channel
quality flag" ;
        product_quality_flag>Note = "The 8-bit quality flags are
channel-specific. Users are advised not to use any scans for which the
highest bit (bit 7) is set to 1. The lowest two bits (bits 0 and 1)
are not used. The meanings of the bits are: bit 7 = Do not use scan
for product generation; bit 6 = Calibration error; bit 5 = Time
sequence error; bit 4 = Earth location questionable; bit 3 =
Brightness temperature out of range; bit 2 = Lunar contamination
warning; bit 1~0 = zero fill;" ;
    } // group Data_Fields

group: Geolocation_Time_Fields {
    variables:
        float latitude_a1_1(nscan, npixel) ;
            latitude_a1_1:standard_name = "latitude" ;
            latitude_a1_1:long_name = "Latitude for AMSU unit A1-1,
e.g., 89.0 GHz" ;
            latitude_a1_1:scale_factor = 1.f ;
            latitude_a1_1:lower_limit = -90.f ;
            latitude_a1_1:upper_limit = 90.f ;
            latitude_a1_1:_FillValue = -999.f ;
            latitude_a1_1:units = "degrees_north" ;
        float latitude_a1_2(nscan, npixel) ;
            latitude_a1_2:standard_name = "latitude" ;
            latitude_a1_2:long_name = "Latitude for AMSU unit A1-2,
e.g., 53.0 GHz" ;
            latitude_a1_2:scale_factor = 1.f ;
            latitude_a1_2:lower_limit = -90.f ;
            latitude_a1_2:upper_limit = 90.f ;
            latitude_a1_2:_FillValue = -999.f ;
            latitude_a1_2:units = "degrees_north" ;
        float latitude_a2(nscan, npixel) ;
            latitude_a2:standard_name = "latitude" ;
            latitude_a2:long_name = "Latitude for AMSU unit A2,
including 23.8 GHz and 31.4 GHz" ;
            latitude_a2:scale_factor = 1.f ;
            latitude_a2:lower_limit = -90.f ;
            latitude_a2:upper_limit = 90.f ;
            latitude_a2:_FillValue = -999.f ;
            latitude_a2:units = "degrees_north" ;
        float longitude_a1_1(nscan, npixel) ;
            longitude_a1_1:standard_name = "longitude" ;
            longitude_a1_1:long_name = "Longitude for AMSU unit A1-1,
e.g., 89.0 GHz" ;
            longitude_a1_1:scale_factor = 1.f ;
            longitude_a1_1:lower_limit = -180.f ;
            longitude_a1_1:upper_limit = 180.f ;
            longitude_a1_1:_FillValue = -999.f ;
            longitude_a1_1:units = "degrees_east" ;
```

```
float longitude_a1_2(nscan, npixel) ;
    longitude_a1_2:standard_name = "longitude" ;
    longitude_a1_2:long_name = "Longitude for AMSU unit A1-2,
e.g. 50.3 GHz" ;
    longitude_a1_2:scale_factor = 1.f ;
    longitude_a1_2:lower_limit = -180.f ;
    longitude_a1_2:upper_limit = 180.f ;
    longitude_a1_2:_FillValue = -999.f ;
    longitude_a1_2:units = "degrees_east" ;
float longitude_a2(nscan, npixel) ;
    longitude_a2:standard_name = "longitude" ;
    longitude_a2:long_name = "Longitude for AMSU unit A2,
including 23.8 GHz and 31.4 GHz" ;
    longitude_a2:scale_factor = 1.f ;
    longitude_a2:lower_limit = -180.f ;
    longitude_a2:upper_limit = 180.f ;
    longitude_a2:_FillValue = -999.f ;
    longitude_a2:units = "degrees_east" ;
char scan_time(nscan, nchar) ;
    scan_time:standard_name = "time" ;
    scan_time:long_name = "Scan start time (UTC) in ISO8601
date/time (YYYY-MM-DD HH-MM-SSZ) format" ;
    scan_time:_FillValue = "0" ;
double scan_time_since98(nscan) ;
    scan_time_since98:standard_name = "time" ;
    scan_time_since98:long_name = "Scan start time (UTC) in a
referenced or elapsed time format" ;
    scan_time_since98:_FillValue = 0. ;
                                scan_time_since98:units =
"seconds since 1998-01-01 00:00:00Z" ;
} // group Geolocation_Time_Fields
}
```